Published in final edited form as:

Immunity. 2019 September 17; 51(3): 491–507.e7. doi:10.1016/j.immuni.2019.08.013.

The transcription factor Bhlhe40 programs mitochondrial regulation of resident CD8+ T cell fitness and functionality

Chaofan Li[1], **Bibo Zhu**[1], **Youngmin Son**[1], **Zheng Wang**[1], **Li Jiang**[1], **Min Xiang**[1], **Zhenqing Ye**[2], **Kathryn E. Beckermann**[3], **Yue Wu**[4], **James Jenkins**[4], **Peter J. Siska**[5,6], **Benjamin G. Vincent**[7], **Y.S. Prakash**[8], **Tobias Peikert**[1], **Brian T. Edelson**[9], **Reshma Taneja**[10], **Mark H. Kaplan**[11], **Jeffrey C. Rathmell**[6], **Haidong Dong**[4], **Taro Hitosugi**[12], **Jie Sun**[1,4]

[1]Department of Medicine, Mayo Clinic, Rochester, MN 55905, USA

[2]Division of Biomedical Statistics and Informatics, Mayo Clinic, Rochester, MN 55905, USA

[3]Division of Hematology/Oncology, Vanderbilt University Medical Center, Nashville, TN 37232, USA

[4]Department of Immunology, Mayo Clinic, Rochester, MN 55905, USA

[5]Internal Medicine III, University Hospital Regensburg, 93042 Regensburg, Germany

[6]Center for Immunobiology, Vanderbilt University Medical Center, Nashville, TN 37232, USA

[7]Lineberger Comprehensive Cancer Center, University of North Carolina, Chapel Hill, NC 27599, USA

[8]Department of Anesthesiology, Mayo Clinic, Rochester, MN 55905, USA

[9]Department of Pathology and Immunology, Washington University School of Medicine, St. Louis, MO 63110, USA

[10]Department of Physiology, National University of Singapore, Singapore 117593

[11]Department of Pediatrics, Indiana University School of Medicine, Indianapolis, IN 46202, USA

[12]Department of Molecular Pharmacology and Experimental Therapeutics, Mayo Clinic, Rochester, MN 55905, USA

SUMMARY

Tissue-resident memory CD8+ T (Trm) cells share core residency gene programs with tumor-infiltrating lymphocytes (TILs). However, the transcriptional, metabolic and epigenetic regulation

Lead contact: Jie Sun, Sun.Jie@mayo.edu.

AUTHOR CONTRIBUTIONS

C.L. performed experiments, analyzed the data and wrote the manuscript; Y.S., B.Z., Z.W., L.J., M.X., J.J. assisted with experiments; K.E.B., P.Y.S., T.P., P.J.S., B.G.V., B.T.E., R.T., T.H., M.H.K., J.C.R., H.D. provided reagents and advice; J.S. supervised the project, designed experiments, and wrote the manuscript.

DECLARATION OF INTERESTS

The authors declare no competing interests.

of Trm cell and TIL development and function is largely undefined. Here, we found that the transcription factor Bhlhe40 was specifically required for Trm cell and TIL development and polyfunctionality. Local PD-1 signaling inhibited TIL *Bhlhe40* expression, and Bhlhe40 was critical for TIL reinvigoration following anti-PD-L1 blockade. Mechanistically, Bhlhe40 sustained Trm cell and TIL mitochondrial fitness and a functional epigenetic state. Building on these findings, we identified an epigenetic and metabolic regimen that promoted Trm cell and TIL gene signatures associated with tissue residency and poly-functionality. This regimen empowered the anti-tumor activity of $CD8^+$ T cells and possessed therapeutic potential even at an advanced tumor stage in mouse models. Our results provide mechanistic insights on the local regulation of Trm cell and TIL function.

Graphical Abstract

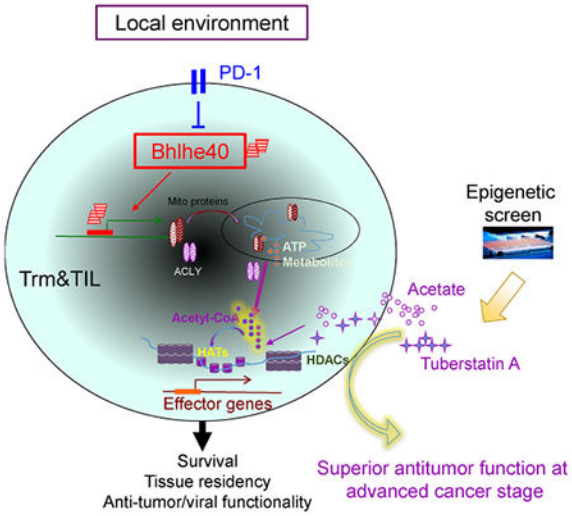

In Brief

The molecular regulation of $CD8^+$ tissue-resident memory (Trm) cells and tumor-infiltrating lymphocytes (TILs) is incompletely understood. *Li et al.* reported that the transcription factor Bhlhe40 was required for Trm cell and TIL mitochondrial fitness and epigenetic programming. They further identified an epigenetic regimen promoting TIL functional program for cancer immunotherapy.

INTRODUCTION

Tissue resident memory $CD8^+$ T (Trm) cells are a recently described population of $CD8^+$ memory T (Tmem) cells, which permanently reside in non-lymphoid tissues (NLT) and rapidly respond to pathogen reinvasion (Ariotti et al., 2014; Kumar et al., 2017; Laidlaw et al., 2014). Generation and maintenance of Trm cells are regulated by a distinct set of transcription factors than those required for circulating Tmem cells, including Runx3, Notch, Blimp-1, Hobbit and Nur77 (Hombrink et al., 2016; Mackay et al., 2016; Milner et al., 2017; Skon et al., 2013). These transcription factors instruct a tissue-residency program that allows for the long-term retention and maintenance of Trm cells within NLT. Trm cells

have elevated expression of a number of effector molecules, including IFN-γ, TNF-α and Granzyme B (GzmB), which enable Trm cells to rapidly respond to stimulation and orchestrate protective immunity (Gebhardt et al., 2009; Jiang et al., 2012). Currently, the transcriptional regulation of "*in situ*" Trm cell functionality (rapid production of a range of effector molecules) is largely unknown. Of note, Trm cells and $CD8^+$ tumor infiltrating lymphocytes (TILs) share a common core residency gene program (Milner et al., 2017). Furthermore, a Trm cell gene signature has been associated with improved patient survival in lung, breast and melanoma cancers (Ganesan et al., 2017; Guo et al., 2018; Savas et al., 2018). However, the mechanisms by which Trm cell and TIL function and fitness are programmed or maintained are incompletely understood.

$CD8^+$ T cell activation, effector differentiation and memory cell formation are closely associated with changes in the cellular metabolic programs. While effector T (Teff) cells mainly use aerobic glycolysis fueling their expansion and effector function, mitochondrial metabolism and oxidative phosphorylation (OXPHOS) are important in supporting Tmem cell maintenance and function (Bantug et al., 2018; Borges da Silva et al., 2018; Buck et al., 2016; Pearce et al., 2009; Sena et al., 2013). Similarly, Trm cells require mitochondria-dependent lipid oxidation for their long-term maintenance (Pan et al., 2017). Mitochondrial energy metabolism and fitness are also required for TIL fitness and function (Scharping et al., 2016; Zhang et al., 2017). However, the transcriptional regulation of mitochondrial metabolism in Trm cells and TILs are largely elusive. In addition to energy generation, mitochondria produce a variety of macromolecules important in cell physiological responses, including the regulation of gene expression (Mehta et al., 2017). For instance, as a critical substrate of histone acetylated modification, Acetyl-CoA is produced following fatty acid or pyruvate oxidation in mitochondria (Peng et al., 2016). Importantly, the increased presence of histone acetylation (such as H3K9 or H3K27 acetylation) and active chromatin state are tightly correlated with the function of $CD8^+$ T cells (Henning et al., 2018). To this end, the suppressive tumor microenvironment (TME) promotes TIL acquisition of a dysfunctional chromatin state in advanced tumor stages (Philip et al., 2017; Sen et al., 2016). The dysfunctional epigenetic programming may limit the efficacy of immunotherapies (Ghoneim et al., 2017). Thus, to achieve effective cancer immunotherapy, it is necessary to re-program the unresponsive T cell epigenetic state within the TME into a functional anti-tumor state.

Bhlhe40 is a stress-responsive transcription factor that is important in a number of cell physiological responses (Ma et al., 2013). Bhlhe40 expression in T helper (Th) cells modulates effector and pathogenic activities of Th1 and Th17 cells (Lin et al., 2016; Yu et al., 2018). Bhlhe40 overexpression in *in vitro* generated "memory" $CD8^+$ T cells results in attenuated recall responses (Hu and Chen, 2013), but the physiological roles of Bhlhe40 in regulating $CD8^+$ Teff and/or Tmem responses remain unclear. Here we demonstrate that Bhlhe40 is specifically required for the development, fitness and polyfunctionality of Trm cells and TILs. Bhlhe40 deficiency leads to impaired production of metabolites required for Acetyl-CoA synthesis, resulting in decreased Trm cell and TIL histone acetylation for the proper expression of functional molecules. Building on the findings, we have identified a regimen that can enhance wildtype (WT) and *Bhlhe40*$^{-/-}$ $CD8^+$ T cell functionality and tissue residency gene programs through *in vitro* screening of an epigenetic library. Our

results provide mechanistic insights on the local regulation of Trm cell and TIL functionality, and offer a viable strategy for developing cancer immunotherapeutic strategies.

RESULTS

Resident CD8$^+$ T cells highly express *Bhlhe40*

To explore Bhlhe40 function in CD8$^+$ T cells, we first determined *Bhlhe40* expression in WT CD8$^+$ T cells following activation. We found that *Bhlhe40* was potently upregulated in CD8$^+$ T cells following activation (Figure S1A). Bhlhe40 was required for sustained expansion and effector molecule production by activated CD8$^+$ T cells *in vitro* (Figures S1B–S1D). Further, there were pronounced differences in the transcriptional profiles between activated WT and *Bhlhe40*$^{-/-}$ CD8$^+$ T cells (4 days post activation, d.p.a.) (Figure 1A).Gene set enrichment analysis (GSEA) showed that Bhlhe40 modulated a core set of tissue signature genes recently discovered to be shared by Trm cells and TILs (Milner et al., 2017), but not gene programs differentiating effector vs. memory or SLEC (short-lived effector cells) vs. MPEC (memory precursor effector cells) (Sarkar et al., 2008) (Figures 1B, S1E, S1F and Table S1). Further, analysis of single-cell RNA sequencing (scRNA-seq) data from human colorectal TILs (Zhang et al., 2018) found that *BHLHE40*^{hi} TILs exhibited enrichment of the core tissue-residency gene signature relative to *BHLHE40*^{low} TILs (Figure 1C).

We next employed an acute influenza virus infection model and a melanoma (B16-F10 expressing chicken ovalbumin (OVA), B16-OVA) transplantation model to study Bhlhe40 function in Trm cell and TIL responses respectively. RNA-seq and prime-flow staining showed that Trm cells and TILs expressed higher *Bhlhe40* compared to their splenic counterparts (Figure 1D and S1G). Moreover, the top 20 *Bhlhe40*-associated genes predicted by the GIANT (Genome-scale Integrated Analysis of gene Networks in Tissues) database (Greene et al., 2015) (Figure S1H) were enriched in both Trm cells and TILs compared to their splenic counterparts (Figure 1E). We compared *BHLHE40* expression in tumor-reactive CD8$^+$ T cells (CD45RO$^+$PD-1$^+$CD11a$^+$) (Dronca et al., 2016) within TILs or peripheral blood mononuclear cells (PBMCs) from renal cell carcinoma (RCC) patients using prime-flow analysis. Tumor-reactive TILs expressed higher *BHLHE40* compared with their paired circulating counterparts (Figure S1I and Figure 1F left). Similarly, human lung Trm (CD103$^+$) cells had increased *BHLHE40* expression than Tmem cells in the PBMCs (Hombrink et al., 2016)(Figure 1F right). In addition, *BHLHE40*-associated genes were enriched in human TILs from colorectal cancer, liver cancer (HCC) and non-small cell lung cancer (NSCLC) compared to CD8$^+$ T cells in the PBMCs (Guo et al., 2018; Zhang et al., 2018; Zheng et al., 2017) (Figure 1G). These data suggest that *Bhlhe40* and its associated genes are highly expressed in both mouse and human resident CD8$^+$ T cells in the NLT or tumors compared to their lymphoid or circulating counterparts.

Intrinsic Bhlhe40 is critical for Trm cell fitness and function

We infected WT or *Bhlhe40*$^{-/-}$ mice with influenza A X31 (H3N2) strain, and examined influenza-specific effector and memory CD8$^+$ T cell responses against MHC-I H2-D^b restricted Nucleoprotein 366-374 peptide (NP$_{366\text{-}374}$). *Bhlhe40*$^{-/-}$ mice exhibited

comparable frequency and numbers of $NP_{366-374}$ Teff cells in the lungs (Teff-Lung) or spleens (Teff-SPL) as those of WT mice at 10 d.p.i. (Figures 2A and S2A). However, Bhlhe40 deficiency caused a marked decrease of frequencies and numbers of lung $CD8^+$ Trm cells (Figures 2B and S2C). The magnitude of the $CD8^+$ lung circulating (Tmem-Cir) or splenic Tmem (Tmem-SPL) cells in *Bhlhe40*$^{-/-}$ mice was comparable as those of WT mice (Figure 2B). Similar decrease of lung $NP_{366-374}$ and $PA_{224-233}$ ($H2\text{-}D^b$-restricted polymerase 224-233 peptide) Trm cell responses was observed in *Bhlhe40*$^{-/-}$ mice following influenza PR8 (H1N1) virus infection (Thomas et al., 2006) (Figures 2C, 2D and S2D). $CD69^+CD103^+$ Trm cells also diminished following X31 or PR8 infection in *Bhlhe40*$^{-/-}$ mice (Figures S2C and S2D). The decreased Trm cell magnitude in *Bhlhe40*$^{-/-}$ mice was associated with enhanced Trm cell apoptosis (Figure 2E).

We next 1:1 mixed WT OTI ($CD90.1^+$) and *Bhlhe40*$^{-/-}$ OTI ($CD90.1^+/CD90.2^+$), and transferred the mixed cells into WT mice. We then infected the mice with influenza PR8 expressing ovalbumin (PR8-OVA) and followed the ratio of WT vs. *Bhlhe40*$^{-/-}$ OTI cells at 10 and 35 d.p.i. (Figure 2F). The ratio of WT to *Bhlhe40*$^{-/-}$ OTI cells remained at ~1:1 in the spleen at the two time points, suggesting that $CD8^+$ T cell-intrinsic Bhlhe40 was dispensable for the generation of splenic Teff and Tmem cells (Figure 2F). Bhlhe40 deficiency caused a modest decrease of OTI effector cells in the lung at 10 d.p.i., but resulted in a marked impairment in the generation of lung Trm cells at 35 d.p.i. (Figures 2F and 2G). Moreover, *Bhlhe40*$^{-/-}$ Trm cells exhibited impairment in the production of IFN-γ (Figures 2H, and S2E). Notably, depletion of circulating $CD8^+$ T cells with low dose anti-CD8 or long-term FTY720 treatment at the memory stage did not alter the ratio of WT vs. *Bhlhe40*$^{-/-}$ Trm cells in the lungs (Figures S2F–S2H). Thus, Bhlhe40 likely acts on tissue-resident $CD8^+$ T cells to promote Trm cell formation, but probably not on recirculating memory T cells recently entering the lungs. To examine whether activated *Bhlhe40*$^{-/-}$ T cells also exhibit defects in Trm cell formation and/or maintenance, we stimulated WT or *Bhlhe40*$^{-/-}$ OTI cells *in vitro* and transferred the effector WT OTI ($CD90.1^+$) and *Bhlhe40*$^{-/-}$ OTI ($CD90.1^+/CD90.2^+$) cells at the ratio of 1:1 into WT mice followed with PR8-OVA infection. Bhlhe40 deficiency in activated $CD8^+$ T cells greatly diminished Trm cell formation, but only modestly affected Tmem-SPL responses (Figure S2I). We also generated T cell-specific Bhlhe40-deficient mice (*Bhlhe40*$^{\Delta T}$) and infected the mice with PR8. T cell-specific deficiency of Bhlhe40 resulted in decreased magnitude of total or $CD69^+CD103^+$ $NP_{366-374}$ and $PA_{224-233}$ lung Trm cells as well as diminished per cell experession of CD103 (Figures 2I, 2J, S2J, S2K and S2L). In addition, both *Bhlhe40*$^{-/-}$ and T cell-specific Bhlhe40 deficiency leaded to marked decrease of the production of effector molecules (IFN-γ, GzmB and TNF) by Trm, but not Tmem-SPL cells (Figures 2K, S2M). Thus, $CD8^+$ T cell-autonomous Bhlhe40 is specifically required for Trm cell formation, fitness and functionality. As a result, *Bhlhe40*$^{-/-}$ mice that were previously infected with X31 exhibited defects in Trm cell-mediated protection against a lethal secondary PR8 challenge in the presence of FTY720, which blocked circulating memory T cell migration to the lungs (Iborra et al., 2016) (Figures 2L). Further, *Bhlhe40*$^{-/-}$ mice that were previously infected with PR8 had defects in Trm cell-mediated protection against secondary X31 challenge (Figures 2M).

Bhlhe40 is vital for TIL fitness and poly-functionality

Trm cells and TILs share a core tissue residency and function gene signature (Milner et al., 2017). To this end, we subcutaneously implanted B16-OVA into WT or *Bhlhe40*$^{-/-}$ mice, and checked TIL responses. *Bhlhe40*$^{-/-}$ mice showed decreased total and antigen-specific (H2-K^{b} OVA$_{257\text{-}264}$ tetramer^{+}) TILs at day 14 and 18 post tumor transplantation (d.p.t.i.) (Figures 3A, 3B, and S3A). *Bhlhe40*$^{-/-}$ TILs had increased apoptosis and decreased IFN-γ and GzmB production (Figures 3C, 3D), yet showed comparable proliferative responses as WT TILs (Figure S3B). In contrast, *Bhlhe40*$^{-/-}$ splenic CD8^{+} T cells exhibit similar levels of apoptosis, IFN-γ or GzmB production as their WT counterparts (Figures 3C and 3D).

T cells capable of producing multiple effector molecules are poly-functional and associated with better cancer control (Yuan et al., 2008; Zhao et al., 2016a). We thus evaluated the poly-functionality of WT and *Bhlhe40*$^{-/-}$ TILs by measuring five effector molecules in TILs (IFN-γ, TNF-α, GzmB, CCL3 and CCL4). *Bhlhe40*$^{-/-}$ TILs showed decreased frequencies of cells simultaneously producing multiple effector molecules (Figures 3E and S3C). Importantly, *Bhlhe40*$^{-/-}$ TILs did not have increased PD-1, TIM-3 or CTLA4 compared to WT TILs (Figure S3D). Notably, “stem-like” TILs (PD-1^{int} TCF1^{+} CXCR5^{+}) expressed much lower *Bhlhe40* than PD-1^{hi} TILs and “exhausted” PD-1^{hi} TIM-3^{+} TILs (Figure S3E), which is consistent with the reported findings that TCF1^{-} TILs have enrichement of Trm cell signature genes and had higher effector molecule expression compared to TCF1^{+} “stem-like” TILs (Kurtulus et al., 2019; Siddiqui et al., 2019). Within the PD-1^{hi} TIM-3^{+} TIL population, *Bhlhe40*^{hi} TILs had higher *Ifng* and enriched with core Trm cell and TIL residency gene signature relative to *Bhlhe40*^{low} TILs (Figures S3F–S3I) (Singer et al., 2016) (Zhang et al., 2018), suggesting that the amount of *Bhlhe40* expression in this TIL population may correlate with their residual function *in situ.* Altogether, our data indicate that Bhlhe40 is key for maintaining TIL function. As a result, *Bhlhe40*$^{-/-}$ mice had increased tumor burden following transplantation with multiple tumor cell lines including B16-OVA, MC-38 (Murine colon adenocarcinoma cells) and LLC (Lewis Lung Carcinoma) (Figures 3F–3H).

We then 1: 1 mixed WT and *Bhlhe40*$^{-/-}$ OTI cells and transferred into B16-OVA bearing mice. While *Bhlhe40*$^{-/-}$ OTI cells competed well with WT OTI cells inside the spleen, Bhlhe40 deficiency resulted in progressive and drastic OTI cell loss inside the tumor, suggesting that intrinsic Bhlhe40 is critical for TIL maintenance during tumor progression (Figures 3I and S3J). Importantly, effector T cell migration to tumor was Bhlhe40-independent (Figure S3K). Further, *Bhlhe40*$^{\Delta T}$ mice exhibited decreased antigen-specific TILs, and diminished CD69 and CD103 expression (Figures 3J, 3K and S3L). TILs from *Bhlhe40*$^{\Delta T}$ mice also showed diminished expression of multiple effector molecules (Figure 3L). Consequently, *Bhlhe40*$^{\Delta T}$ mice had enhanced tumor growth (Figure 3M). Conversely, ectopic *Bhlhe40* expression in OTI cells facilitated T cell accumulation inside tumor and decreased B 16-OVA tumor burden (Figures 3N–3O and S3M–S3N). Thus, T cell-intrinsic Bhlhe40 is essential for TIL residency, fitness and function.

Bhlhe40 deficiency abrogated the therapeutic effects of anti-PD-L1 blockade

A number of the mediators including IL-1β, TNF, PGE2 and IL-15 promoted *Bhlhe40* expression in $CD8^+$ T cells (Figure S4A). Further, CD28 co-stimulation boosted *Bhlhe40* expression in $CD8^+$ T cells (Figure S4B). It is thus possible that one or multiple of these factors could promote *Bhlhe40* expression in NLT and/or tumors *in vivo.* Recent advances in anti-PD (PD-1 or PD-L1 blockade) therapy have revolutionized cancer treatment (Dong et al., 2002; Topalian et al., 2012), although the mechanisms underlying the efficacy of anti-PD blockade are still incompletely defined. We hypothesized that PD-L1-PD-1 interaction may inhibit *Bhlhe40* expression within TME to dampen TIL effector activity *in situ.* To explore the idea, we transplanted B16-OVA into both flanks of WT mice, then injected either anti-PD-L1 or control IgG intratumorally into the bi-lateral tumors from 5 d.p.t.i. (Figure 4A). Local PD-L1 blockade decreased tumor size and increased *Bhlhe40* expression in TILs (Figures 4A, S4C), suggesting that PD-1 signaling suppresses TIL *Bhlhe40* expression *in situ*. Importantly, co-transfer of congenically distinct WT and $Pdcd1^{-/-}$ OTI cells demonstrated that $CD8^+$ T cell-intrinsic PD-1 signaling suppressed *Bhlhe40* expression in TILs (Figure S4D). Anti-PD-L1 treatment increased TIL survival and IFN-γ production in WT mice (Figures 4B, 4C). However, Bhlhe40 deficiency abrogated the effects (Figures 4B, 4C). In accordance, α-PD-L1 controlled tumor growth in WT mice, but not in $Bhlhe40^{-/-}$ mice (Figures 4D, S4E). T cell-specific Bhlhe40 deficiency also abrogated T cell reinvigoration and the therapeutic effects of α-PD-L1 treatment (Figures 4E–4G). These data indicate that local PD-1 signaling suppresses *Bhlhe40* expression in TILs, and Bhlhe40 is critical for TIL reinvigoration and therapeutic efficacy of anti-PD therapy.

Bhlhe40 directs mitochondrial regulation of Trm cell and TIL active chromatin status

We next performed RNA-seq analysis on WT and $Bhlhe40^{-/-}$ OTI Trm cells isolated from PR8-OVA infected mice. Bhlhe40 was required for modulating the expression of a large number of Trm cell-associated genes (Figures S5A, S5B). Nanostring analysis confirmed that Bhlhe40 was needed for the expression of genes necessary for Trm cell formation and/or maintenance including *Runx3* and *Notch 1, 2* (Hombrink et al., 2016; Milner et al., 2017) (Figures S5C, D). Notably, the expression of immune-associated genes was relatively similar between WT and $Bhlhe40^{-/-}$ Tmem-SPL cells, indicating that Bhlhe40 "preferentially" regulates Trm cell function (Figures S5C and S5D). Pathway analysis of the genes downregulated in $Bhlhe40^{-/-}$ Trm cells (compared to WT Trm cells) revealed that the mitochondrion was the primary target of *Bhlhe40*-directed gene expression (Figure 5A). $Bhlhe40^{-/-}$ Trm cells had diminished expression of genes encoding components of mitochondrial membrane or genes involved in mitochondrial metabolism and/or OXPHOS, which are vital for fueling Tmem cells and TILs (Pearce et al., 2009; Scharping et al., 2016) (Figures 5B, S5E). Consistently, analysis of scRNA-seq data from mouse (Singer et al., 2016) and human (Zhang et al., 2018) PD-1^{hi} TIM-3^+ $CXCR5^-$ TIL population, which express considerable amount of *Bhlhe40,* has revealed that $Bhlhe40^{hi}$ TILs had enrichment of OXPHOS genes relative to $Bhlhe40^{low}$ TILs (Figures S5R). Bhlhe40 deficiency resulted in decreased expression of a number of nuclear-encoded electron transport genes (Figure 5 C). Chromatin immunoprecipitation (ChIP) experiments confirmed that Bhlhe40 directly bound to mitochondrial genes in both $CD8^+$ and $CD4^+$ T cells (Figure 5D, S5F) (Huynh et al., 2018). Thus, Bhlhe40 functions to promote mitochondrial gene transcription in Trm

cells. Consistently, *Bhlhe40*$^{-/-}$ Trm cells exhibited lower oxygen consumption rate (OCR), but not extracellular acidification rate (ECAR) (Figure 5E). Electron microscopic analysis revealed that both *Bhlhe40*$^{-/-}$ Trm cells and TILs had enhanced mitochondrial damage (Figures 5F and 5G). *Bhlhe40*$^{-/-}$ TILs also had lower OCR (Figure S5G). In contrast, WT Tmem-SPL and *Bhlhe40*$^{-/-}$ Tmem-SPL cells expressed comparable amounts of mitochondrial genes and had similar mitochondrial morphology (Figure 5F and S5H).

Beyond OXPHOS, mitochondria play key roles in biosynthesis and epigenetic regulation of gene expression (Mehta et al., 2017). To this end, we employed an *in vitro* dendritic cell (DC) and T cell culture model to examine the downstream metabolic and epigenetic consequences of dysfunctional mitochondria in *Bhlhe40*$^{-/-}$ T cells. We confirmed that Bhlhe40 was required for the maintenance of CD8^{+} T cell mitochondrial fitness and metabolism in the *in vitro* model as *Bhlhe40*$^{-/-}$ CD8^{+} T cells showed diminished OCR, damaged mitochondria compared to their WT counterparts at 4 d.p.a. (Figures S5I and S5J). As a result, *Bhlhe40*$^{-/-}$ CD8^{+} T cells had lower cellular ATP concentration than WT CD8^{+} T cells at 4 d.p.a. (Figure S5K). We then measured more than 400 metabolites in WT and *Bhlhe40*$^{-/-}$ CD8^{+} T cells at 4 d.p.a. by Quadrupole Time-of-Flight Mass Spectrometry (QTOF/MS). This metabolomics analysis revealed that there was a reduction of metabolites in the tricarboxylic acid (TCA) cycle, butanoate metabolism, amino acid (AA) and pyruvate metabolic pathways in *Bhlhe40*$^{-/-}$ CD8^{+} T cells compared to WT CD8^{+} T cells (Figure 5H). Quantitative measurement of TCA metabolites by Gas chromatography–mass spectrometry (GC/MS) confirmed that *Bhlhe40*$^{-/-}$ T cells had a global decrease in TCA metabolites (Figure 5I). Of note, stable isotope tracer analysis (SITA) analysis found that there were no significant defects for the synthesis of citrate pools from incorporated pyruvate or glutamine in *Bhlhe40*$^{-/-}$ CD8^{+} T (Figure S5L), but the pyruvate uptake was relatively decreased in *Bhlhe40*$^{-/-}$ CD8^{+} T cells (Figure S5M), which is consistent with the diminished pyruvate transporter gene (*Slc16a1*) expression in *Bhlhe40*$^{-/-}$ CD8^{+} T cells (Figure S5N).

Those downregulated metabolic pathways (TCA, butanoate and AA metabolisms) and ATP are important in the biosynthesis of Acetyl-CoA, a critical substrate of histone acetylation that is required for the active chromatin state in cells (Wellen et al., 2009). Indeed, *Bhlhe40*$^{-/-}$ CD8^{+} T cells showed lower cellular Acetyl-CoA concentration compared to WT CD8^{+} T cells (Figure 5J). Consequently, total acetylated H3 was decreased in cultured *Bhlhe40*$^{-/-}$ CD8^{+} T cells (Figure 5K). Importantly, *Bhlhe40*$^{-/-}$ Trm cells and TILs exhibited diminished acetylated H3 compared to their WT counterparts (Figure 5K). Thus, Bhlhe40 deficiency decreased cellular Acetyl-CoA concentration and histone acetylation in CD8^{+} T cells, which likely caused the impaired expression of effector molecules and defective anti-viral and antitumor functionality *in vivo.* Conversely, ectopic *Bhlhe40* expression modestly increased mitochondrial respiratory chain gene expression and promoted histone H3 acetylation (Figures S5P and S5Q), indicating that Bhlhe40 may determine histone acetylation in the functional gene loci of CD8^{+} T cells. In accordance, we observed marked decrease of acetyl H3K9 and acetyl H3K27 in the *Ifng* locus in *Bhlhe40*$^{-/-}$ CD8^{+} T cells (Figure 5L). We also noticed decreased acetyl H3K27 in the loci of mitochondrial complex genes (*Cox6a1* and *Atp5e*) (Figure S5O). Taken together, these data indicate that Bhlhe40 is critical for the maintenance of Trm cell and TIL mitochondrial fitness and function, thereby promoting active chromatin modifications for their *in situ* functionality.

Identification of an epigenetic regimen promoting a CD8+ T cell residency and functional program

We reasoned that the provision of extra TCA intermediates such as pyruvate or citrate may restore IFN-γ production by *Bhlhe40*$^{-/-}$ CD8^{+} T cells through the promotion of Acetyl-CoA production and histone acetylation. However, extra TCA intermediate supplementation, including pyruvate, citrate, methyl-pyruvate (MP) and dimethyl-alpha ketoglutarate (DMK) failed to promote IFN-γ production by *Bhlhe40*$^{-/-}$ CD8^{+} T cells (Figures S6A and S6B), suggesting that diminished cellular citrate concentration may not be the primary reason for the impaired IFN-γ production in *Bhlhe40*$^{-/-}$ T cells. To this end, ATP citrate lyase (ACLY) is required for Acetyl-CoA production from citrate (Wellen et al., 2009). Consistent with the inability of pyruvate or citrate to rescue *Bhlhe40*$^{-/-}$ CD8^{+} T cell IFN-γ production, *Bhlhe40*$^{-/-}$ CD8^{+} T cells had diminished expression of ACLY (Figures S6C, S6D). These data suggest that direct targeting the downstream epigenetic machinery may be a viable approach to rescue IFN-γ production by *Bhlhe40*$^{-/-}$ CD8^{+} T cells. To this end, we sought to identify epigenetic modifiers that can directly stimulate IFN-γ production in activated CD8^{+} T cells. To do this, we activated IFN-γ-YFP CD8^{+} T cells *in vitro* and screened an epigenetic library to identify chemicals that can promote IFN-γ expression in activated T cells (Figure 6A). A few chemicals, mainly histone deacetylase inhibitors (HDACi), especially Tubastatin A (TA) could promote IFN-γ production with low cellular toxicity, although a large number of other HDACi failed to do so, demonstrating a unique effect of TA (Figures 6A, 6B). Notably, TA promoted, but did not fully restore IFN-γ production by *Bhlhe40*$^{-/-}$ CD8^{+} T cells (Figure S6E). We reasoned that the supplementation of acetate (Ac), which is a TCA cycle-independent substrate for Acetyl-CoA synthesis (Zhao et al., 2016b), could further boost histone acetylation and cytokine production by *Bhlhe40*$^{-/-}$ CD8^{+} T cells. Indeed, TA and Ac cooperatively enhanced IFN-γ production by *Bhlhe40*$^{-/-}$ CD8^{+} T cells (Figure 6C). However, TA combined with other metabolic substrates such as pyruvate and citrate failed to do so (Figure S6F).

TA and Ac cooperatively promoted WT or *Bhlhe40*$^{-/-}$ CD8^{+} T cell poly-functionality and the expression of a number of cytokines and cytotoxic molecules (Figure 6D and 6E). Furthermore, TA/Ac treatment increased CD69 and CD103 expression, and a large number of genes associated with Trm cell and TIL formation and residency programs in both WT and *Bhlhe40*$^{-/-}$ CD8^{+} T cells (Figures 6F, 6G and S6G). Moreover, those upregulated genes following TA/Ac treatment showed enrichment in WT Trm cells compared to *Bhlhe40*$^{-/-}$ Trm cells (Figure S6H). Thus, we have identified a metabolic and epigenetic regimen capable of promoting the Bhlhe40-dependent CD8^{+} T cell residency and functionality gene programs. Consistent with this idea, TA/Ac treatment resulted in increased histone H3 acetylation and increased H3K9 acetylation in *Ifng, Gzmb* and *Itgae* (CD103) loci in CD8^{+} T cells (Figures 6H and 6I).

Epigenetic modification of resident CD8+ T cell functionality promotes superior tumor control

We reasoned that the epigenetic modification of CD8^{+} T cell residency and functionality programs by TA/Ac treatment may empower *Bhlhe40*$^{-/-}$ CD8^{+} T cell antitumor activities. To this end, B16-OVA bearing mice were adoptively transferred with WT or *Bhlhe40*$^{-/-}$

effector OTI cells at 6 d.p.t.i. Compared to WT effector OTI cells, *Bhlhe40*$^{-/-}$ OTI cells failed to control tumor growth (Figure 7A). However, TA/Ac treatment enabled *Bhlhe40*$^{-/-}$ OTI cells to inhibit tumor growth (Figures 7A, S7A), suggesting that TA/Ac treatment reinvigorated *Bhlhe40*$^{-/-}$ CD8^{+} T cell antitumor activities. The progressive growth of tumor is accompanied with enhanced immunosuppression to effector T cells by TME (Rabinovich et al., 2007; Scharping et al., 2016). Consistent with the idea, even WT effector OTI cells had limited therapeutic efficacy when transferred into mice with a large tumor burden at 10 or 12 d.p.t.i. (> 120 mm^2), which was in sharp contrast to results of WT effector OTI transfer at 6 d.p.t.i. (Figures 7A, 7B, S7B and S7C). We reasoned that the direct modulation of CD8^{+} epigenetic status by TA/Ac treatment may empower WT CD8^{+} T cell anti-tumor functionality under the strong immunosuppression rendered by TME at the advanced tumor stage. Consistent with this hypothesis, TA/Ac treatment potentiated WT effector OTI cells to control tumor growth even at these advanced tumor stages (Figures 7B, S7B and S7C).

TILs develop a fixed dysfunctional chromatin state at advanced tumor stages, which diminishes their anti-tumor capability (Philip et al., 2017). Therefore, to provoke TIL function, we injected TA/Ac intratumorally at 11 d.p.t.i. following B16-OVA transplantation, when tumor area is larger than 100 mm^2. TILs showed increased histone H3 acetylation following TA/Ac treatment *in vivo* (Figures 7C, S7D), indicating that TA/Ac may at least partially reverse inaccessible chromatin states of dysfunctional TILs (Henning et al., 2018). Further, TA/Ac treatment augmented IFN-γ and CCL3 production by TILs (Figure 7D). PD-1 blockade shows limited effects in reversing the dysfunctional chromatin states in exhausted CD8^{+} T cells (Pauken et al., 2016). This epigenetic fate inflexibility of TILs may limit the efficacy of anti-PD immunotherapies (Pauken et al., 2016). Consistent with the concept, anti-PD-L1 treatment inhibited tumor growth when inoculated at 5 d.p.t.i. (Figure S4C), but failed to do so when inoculated at 11 d.p.t.i. (Figure 7E). TA/Ac treatment promoted tumor control in mice with a large tumor burden at 11 d.p.t.i. (Figure 7E). Furthermore, TA/Ac treatment showed efficacy to control MC-38 tumor growth when inoculated at 15 d.p.t.i. (tumor > 100 mm^2) (Figure 7F). TA/Ac treatment did not exhibit synergistic effects with anti-PD therapy (Figure S7E), supporting the view that TA/Ac may target the downstream pathways of anti-PD therapy. We have also implanted B16-OVA tumor to both flanks of the mouse and treated the bi-lateral tumors with TA/Ac or vehicle at 10 d.p.t.i. Local treatment of TA/Ac resulted in smaller sizes of tumor compared to the distal tumor received vehicle treatment in the same WT mouse (Figure 7G), suggesting that TA/Ac treatment likely targets TILs directly rather than circulating CD8^{+} T cells to control tumor growth. We performed similar treatment regimen in *Bhlhe40*$^{\Delta T}$ mice (Figure 7H). TA/Ac treatment promoted Trm cell-like TIL (CD69^{+}CD103^{+}) presence, mitochondrial gene expression and histone H3 acetylation in Bhlhe40-deficient TILs (Figures S7F–S7H). Consistently, TA/Ac treatment lowered tumor burden compared to the distal tumor received vehicle treatment in the same mouse (Figure 7H and S7I). Importantly, CD8^{+} T cell depletion largely abolished the efficacy of TA/Ac treatment (Figure 7I), suggesting that TA/Ac promoted CD8^{+} T cell-dependent tumor control at the advanced cancer stage. Although it is still possible that the direct tumoricidal effects of TA may contribute to the therapeutic effects of TA/Ac treatment.

DISCUSSION

Here we have shown that Bhlhe40 maintains Trm cell and TIL mitochondrial fitness and metabolism, thereby promoting an active chromatin state for Trm cell and TIL residency and functionality. An important question is why Bhlhe40 specifically affects tissue-resident $CD8^+$ T cell function over circulating $CD8^+$ T cells. This could be linked to the higher expression of *Bhlhe40* in Trm cells and TILs compared to their circulating counterparts. In addition, tissue or tumor microenvironment may further provoke $CD8^+$ T cells relying on Bhlhe40 for their survival and function. Mucosal tissues and tumors have limited nutrients (such as glucose) and/or under hypoxic or oxidative conditions (Chang et al., 2015; Colgan et al., 2016). These local environments would likely cause stresses to resident T cells that originate from nutrient-rich or less stressful lymphoid organs. As a stress responsive protein, Bhlhe40 is likely only required for the survival and function of $CD8^+$ T cells under stress conditions.

Mitochondrial fitness in TILs is dampened compared to their circulating and secondary lymphoid compartments (Scharping et al., 2016). In the absence of Bhlhe40, TIL mitochondria damage was further exacerbated, suggesting that Bhlhe40 is critical for maintaining the residual function of mitochondria in TILs. Recent evidence has revealed marked cellular heterogeneity within TILs (Azizi et al., 2018; Li et al., 2019). Notably, a population of stem-like $TCF1^+$ TILs has been demonstrated to be important in mediating the proliferative response to anti-PD therapy (Kurtulus et al., 2019; Siddiqui et al., 2019). We found that $TCF1^+$ TILs expressed lower amount of *Bhlhe40* compared to PD1 ^{hi} or PD-1^{hi} TIM-3 $^+$ TILs. These data are consistent with the results that $TCF1^-$ TILs exhibit Trm cell-gene program and express higher *Ifng* and *GzmB* compared to the stem-like $TCF1^+$ TILs (Kurtulus et al., 2019; Siddiqui et al., 2019). Thus, Bhlhe40 may be selectively important for the fitness and function of $TCF1^-$ Trm-like TILs (Savas et al., 2018; Siddiqui et al., 2019). In support, *Bhlhe40* expression in both mouse and human PD-1^{hi} TIM-3^+ $CXCR5^-$ TILs positively correlated with *Ifng* expression, tissue residency and mitochondrial metabolism gene signatures. Thus, there may be further phenotypic and functional heterogeneity within this “exhausted” TIL population as defined by the amount of *Bhlhe40* expression. Among these TILs, *Bhlhe40*^{hi} cells may represent “true” Trm-like TILs that still possess residual mitochondrial function and exhibit anti-tumor effector activities *in situ.* Further revitalization of Bhlhe40-dependent mitochondrial function and effector activities in Trm-like TILs is likely a key for effective cancer immunotherapy.

$CD8^+$ TILs progressively develop a fixed dysfunctional chromatin state in advanced tumor stages and TIL epigenetic inflexibility may limit the efficacy and durability of anti-PD therapies (Philip et al., 2017). Consistent with the idea, we found that PD-L1 blockade failed to provide therapeutic effects when inoculated at the advanced tumor stages. To tackle this major barrier of anti-PD therapy, we have employed *in vitro* functional screening and identified an epigenetic regimen that is capable of reinvigorating TIL antitumor function in large tumors, potentially through direct targeting on the TIL epigenetic state. Thus, epigenetic targeting on TIL function may represent a promising strategy to overcome tumor anti-PD resistance. In our screen, Tubastatin A represents a fairly unique HDAC inhibitor that promoted IFN-γ production by activated $CD8^+$ T cells without causing overt cell death.

Tubastatin A is a potent HDAC6 inhibitor but also possesses inhibitory activities against HDAC8 (M et al., 2016). It is possible that Tubastatin A functions to inhibit HDAC6 activity to promote $CD8^+$ T cell function in our setting. However, HDAC6-deficient $CD8^+$ T cells express comparable amount of IFN-γ as WT $CD8^+$ T cells (Nunez-Andrade et al., 2016). Thus, Tubastatin A may target both HDAC6 and HDAC8 to increase $CD8^+$ T cells effector function. Of note, the provision of acetate, which is a substrate supporting Acetyl-CoA synthesis even in the absence of ACLY (Peng et al., 2016; Zhao et al., 2016b), cooperated with Tubastatin A to further enhance $CD8^+$ T cell residency and poly-functionality gene programs *in vitro.* Likewise, emerging data have suggested that acetate and other short chain fatty acid may promote $CD8^+$ T cell metabolism and function (Balmer et al., 2016; Qiu et al., 2019; Trompette et al., 2018).

Even though TA/Ac treatment improves $CD8^+$ T cell effector function, the treated tumors still steadily progress albeit at a slower rate than tumors receiving vehicle control. It is possible that epigenetic targeting in TILs alone is not sufficient to achieve complete tumor regression, which would suggest that regimens that can increase continuous $CD8^+$ T cell infiltration to the tumor may be needed to achieve superior tumor control. Tumor cells may also develop many adaptive resistance strategies to promote their growth even with strong immune activation (Hamieh et al., 2019; Poggio et al., 2019; Ribas, 2015; Sharma et al., 2017). Notably, TA/Ac treatment not only enhances *Bhlhe40*$^{-/-}$ $CD8^+$ T cell effector and resident gene expression but also promotes the expression of these genes in WT $CD8^+$ T cells (albeit to a lesser extent), suggesting that TA/Ac does not selectively target on *Bhlhe40*$^{-/-}$ $CD8^+$ T cells. In addition, direct manipulation of $CD8^+$ T cell epigenetic state by TA/Ac likely will not completely reverse the multiple defects of mitochondrial function and metabolism caused by Bhlhe40 deficiency. Future studies are required to determine the extent of rescue of TA/Ac treatment in revoking impaired *Bhlhe40*$^{-/-}$ Trm cell and TIL responses, particularly on Trm cell and TIL long-term persistence *in vivo.* Nevertheless, the appropriate combinations of epigenetic modifiers with certain metabolites may represent promising approaches for maximally reinvigorating tissue or tumor-resident $CD8^+$ T cell antiviral or antitumor activities.

Overall, we have identified a mechanism for programming the mitochondrial and epigenetic regulation of resident $CD8^+$ T cell functionality *in situ.* This mechanism is critically important in the antiviral and antitumor activities of Trm cell and TILs respectively. Building on these findings, we propose a potential metabolic and epigenetic modality to activate a functional $CD8^+$ T cell residency gene signature that mediates effective cancer immunotherapy at an advanced tumor stage.

STAR Methods

LEAD CONTACT AND MATERIALS AVAILABILITY

Further information and requests for resources and reagents should be directedto and will be fulfilled by the Lead Contact (sun.jie@mayo.edu).

Method Details

Mice, infection and tumor transplantation: Mice on a C57BL/6 background were used in this study. *Bhlhe40*$^{-/-}$ mice were originally generated previously as reported (Sun et al., 2001). *Bhlhe40*$^{tm1a(KOMP)Wtsl}$ mice were obtained from MMRRC and were crossed to FLP delete strain (JAX) mice to generate *Bhlhe4d*$^{fl/l}$ mouse strain. *Bhlhe40*$^{f/l}$ mice were then crossed with CD4-cre mice (JAX) to generate *Bhlhe40*^{Kl} mice. IFN-γ-YFP (GREAT) reporter mice, OTI Thyl.1 mice and C57BL/6 mice were obtained from the Jackson Laboratory. Thy1.1$^+$ Thy1.2$^+$ *Bhlhe40*$^{-/-}$ OTI mice were generated by crossing *Bhlhe40*$^{-/-}$ mice with Thy1.1$^+$ OTI mice. Thy1.1$^+$ Thy1.2$^+$ *Pdcd1*$^{-/-}$ OTI mice were generated by crossing *Pdcd1*$^{-/-}$ mice with Thy1.1$^+$ OTI mice. All animal protocols were approved by the Institutional Animal Care and Use Committees (IACUC) of the Mayo Clinic or the Indiana University School of Medicine. Influenza A/PR8/34 (~200 pfu/mouse in the primary infection and ~1χ10^4 pfu/mouse in the secondary infection), recombinant PR8 expressing Ovalbumin SINNFEKL peptide (PR8-OVA) (~500 pfu/mouse) and Influenza A X31 (~800 pfu/mouse in the primary infection and ~8χ10^4 pfu/mouse in the secondary infection) infection were performed by intranasal (i.n.) under anesthesia as described before (Sun et al., 2009).

Cell Lines and tumor implantation: Tumor cell lines were from the laboratory of Haidong Dong and reported before (Dronca et al., 2016; Tang et al., 2018), including B16-OVA melanoma, Lewis lung carcinoma (LLC), and MC38 colon adenocarcinoma. B16-OVA cell line and MC38 cell line were cultured in RPMI-1640 with 20mM HEPES and 10% FBS. The LLC cell line was cultured in DMEM with 20mM HEPES and 10% FBS. Tumor cells (B16-OVA, LLC and MC38) were subcutaneously injected into the flank of mice (5 χ 10^5 cells/mouse). Tumor size was measured every 2 days starting from day 6. Tumor size was calculated as length χ width. Mice with tumor size larger than 400 mm^2 or ulcerative were euthanized and counted as mortality.

Intravascular CD8$^+$ T cell labeling for identification of Trm cells: Mice were injected i.v. with 1.5 μg of anti-CD45 diluted in 200 μL of sterile PBS as previously described (Anderson et al., 2014). Mice were euthanized and tissues were collected five minutes after injection of the i.v. Ab. Tissues were dissociated in 37°C for 30 min with Gentle-MACS (Miltenyi). Lung circulating CD8$^+$ T cells are i.v. Ab$^+$ and lung-resident CD8$^+$ T cells are defined by i.v. Ab$^-$.

T cell adoptive transfer: For WT OTI T cell transfer, Thy1.1 WT OTI cells were purified via CD8a-microbeads (Miltenyi). 5 χ 10^4 cells were transferred into C57BL6 mice. For competition experiment, wild-type and *Bhlhe40*$^{-/-}$ OTI cells were mixed as ratio of 1:1, and were adoptive transferred into recipient mice subsequently infected with PR8-OVA (1 χ 10^5 mixed cells / mouse), or were transferred into B16-OVA bearing mice (2 χ 10^6 mixed cells / mouse).

Quantitative RT-PCR: Total RNA were extracted from cells as indicated in the text with Total RNA purification kit (Sigma) and treated with DNase I (Invitrogen). Random primers and MMLV reverse transcriptase (Invitrogen) were used to synthesize first-strand cDNAs

from equivalent amounts of RNA from each sample. These cDNA was subjected to realtime-PCR with Fast SYBR Green PCR Master Mix (Applied Biosystems). qPCR was conducted in duplicates in QuantStudio3 (AppliedBioscience). Data were generated with the comparative threshold cycle (Delta CT) method by normalizing to hypoxanthine phosphoribosyltransferase (HPRT). *Bhlhe40* primers were purchased from IDT (Assay ID. Mm.PT.58.10417747). Sequences of primers used in the studies are listed as following. Primer sequences: *Hprt-F:* CTCCGCCGGCTTCCTCCTCA, *Hprt-*R:ACCTGGTTCATCATCGCTAATC. *Acly*-F: TTCGTCAAACAGCACTTCC, *Acly-R:* ATTTGGCTTCTTGGAGGTG.

Tumor and lung tissue dissociation: Tumor tissues were harvested and weighed at indicated days after implantation. Tumor tissues were dissociated into single cell suspension by GentleMACS (Miltenyi Biotech) following the instruction of mouse Tumor Dissociation Kit (Miltenyi). Spleens were also isolated and dissociated into single cell suspension using 70 μm cell strainer (BD Biosciences). Lung tissues were harvested and digested with Collagenase Type 2 for 30 min as described previously (Yao et al., 2015).Tumor, lung and spleen single cell suspension were further passed through 70pm cell strainer one time before next step operation.

$CD8^+$ T cell culture *in vitro*: Bone marrow-derived dendritic cells (BMDC) were differentiae *ex vivo* in the presence of GM-CSF (20ng/ml) for 6 days as described(Sun and Pearce, 2007). $CD8^+$ T cells were purified from spleen and lymph nodes with the CD8a (Ly-2) MicroBeads (Miltenyi Biotech). The purified $CD8^+$ T cells were cocultured with BMDC as the ratio of 10:1 (T:DC) in round bottom 96-well plate, and were stimulated with soluble anti-CD3 (1 μg/ml) as described before(Sun et al., 2011). For cytokines stimulation, IL-1 β (10 ng/ml), IL-15 (20 ng/ml), IL-21 (10 ng/ml), IL-7 (10 ng/ml), IL-33 (10 ng/ml), TNF (10 ng/ml), TGFβ (10 ng/ml), IL-10 (10 ng/ml) and PGE2 (2 μM) were added in to the co-culture system. For anti-CD28 stimulation, purified $CD8^+$ were stimulated with plat-bound anti-CD3 (2 μg/ml), soluble anti-CD28 (10 μg/ml) were presented into the culture system. For metabolites and HDACi treatment, in vitro cultured $CD8^+$ T cells were treated with pyruvate (1mM), citrate (5mM), methyl-pyruvate (MP) (1mM) and dimethyl-alpha ketoglutarate (DMK) (1mM), acetate (20mM) and Tubastatin A (10 μM) at 3 d.p.a. and cytokine production were measured at 4 d.p.a.

Retroviral Transduction: $CD8^+$ T cells were stimulated with α-CD3 and α-CD28. At day 1 of the culture, cells were transduced with retroviruses (Lin et al., 2014) through spin infection (2,500 rpm, 90 min) in the presence of 5μg/ml polybrene as previously described (Yao et al., 2013). After transduction, cells were analyzed by flow cytometry, and transferred into B16-OVA bearing recipients (5 d.p.t.i.) on day 2 post transduction.

Polyfunctional T cell analysis: Single cell suspension were stimulated with PMA (0.1 μg/ml) and Ionomycin (1 μg/ml) (Sigma) or OVA257-264 peptide (Anaspec, 1 μg/ml) or $NP_{366-374}$ peptide (Anaspec,1 μg/ml) for 5h in the presence of 2μM monensin (BD Biosciences), and then stained with APC-CY7 conjugated anti-CD8. Cells were fixed and permeabilized by fixation buffer and intracellular staining perm wash buffer (Biolegend),

and stained with anti-IFN-γ, anti-MIP-1α, anti- MIP-β, anti- TNF-α, and anti-GzmB as described(Yao et al., 2013). Then Boolean gates were applied to analyze (Precopio et al., 2007).

Cell sorting: Tumor infiltrated $CD8^+$ T cells were purified with the CD8a (Ly-2) MicroBeads (Miltenyi Biotech), and then were stained with Percp/CY5.5 conjugated anti-CD3, APC conjugated anti-CD8β, BV421 conjugated anti-CD44, $CD3^+$ $CD8^+$ $CD44^+$ or $CD3^+$ $CD8^+$ $CD44^-$ cells were sorted by BD FACSAria II. For OTI Trm cell sorting, 1.5 μg FITC conjugated anti-CD45 mice were injected i.v. 5 minutes before mice were scarified. OTI cells were enriched by CD8a (Ly-2) MicroBeads (Miltenyi Biotech), and stained with BV421 conjugated anti-CD8a, APC conjugated anti-CD90.1, and PE conjugated anti-CD90.2. Trm cells were sorted based on (i.v. $CD45^-$) $CD8^+CD90.1^+CD90.2^-$ or (i.v. $CD45^-$) $CD8^+CD90.1^+CD90.2^+$.

Chromatin Immunoprecipitation: 10×10^6 activated wild-type or *Bhlhe40* deficient $CD8^+$ T cells were cross linked with 1% formaldehyde and lysed by sonication (Yao et al., 2013). Cell lysis were incubated with Anti-Histone H3 (acetyl K27) (2 μg/sample), Anti-Histone H3 (acetyl K9) (2 μg/sample), BHLHE40 antibody (10 μg/sample) or normal rabbit IgG. The immunocomplexes were precipitated with Protein A agarose beads at 4°C for 2 hr, washed, and eluted and cross-links were reversed at 65°C overnight. DNA was purified and prepared for realtime PCR. Primer sequence: *Cox6a1-F:* ggtgctgtcagcgtctcggg, *Cox6a1*-R: cgggtacctgaaccctcctcg. *Mrps16-F:* cgtccgcaccactccagagcc, *Mrps16-R:* gtagcagtcaaggatcagtc. *Atp5e-F:* tttgcaatgtggttccatcg, *Atp5e*--R: tcgagcccgctctgagtgac, *GzmB-F:* ctgaatgctctccgctccct, *GzmB-R:* gagtttggggtgaggggaaa, *Itgae-F:* acttctggaagacagaaacc, Itgae-R: caggcgggtctcagtgagtc, and as described previously (Kanda et al., 2016; Peng et al., 2016).

Seahorse analysis: Oxygen consumption rates (OCR) and extracellular acidification rates (ECAR) were measured with XFe-24 or XF-P Extracellular Flux Analyzers (Seahorse Bioscience). Briefly, sorted $CD8^+$ T cells were planted to the Cell-Tak (3.3 ug/well) coated XF 24-well plate or XF 8-well plate, OCR and ECAR were testing in the presence of oligomycin (1 μM), FCCP (1 μM), rotenone/antimycin A (0.5 μM) orderly.

RNA-seq: RNA from Sorted $CD8^+$ T cells was extracted using an RNeasy kit (Qiagen) following the manufacturer's instructions. After quality control, High quality total RNA was used to generate the RNA sequencing library. cDNA synthesis, end-repair, A-base addition, and ligation of the Illumina indexed adapters were performed according to the TruSeq RNA Sample Prep Kit v2 (Illumina, San Diego, CA). The concentration and size distribution of the completed libraries was determined using an Agilent Bioanalyzer DNA 1000 chip (Santa Clara, CA) and Qubit fluorometry (Invitrogen, Carlsbad, CA). Paired-end libraries were sequenced on an Illumina HiSeq 4000 following Illumina's standard protocol using the Illumina cBot and HiSeq 3000/4000 PE Cluster Kit. Base-calling was performed using Illumina's RTA software (version 2.5.2). Paired-end RNA-seq reads were aligned to the mouse reference genome (GRCm38/mm10) using RNA-seq spliced read mapper Tophat2 (v2.1.1). Pre- and post-alignment quality controls, gene level raw read count and ormalized

read count (i.e. FPKM) were performed using RSeQC package (v2.3.6) with NCBI mouse RefSeq gene model. RNA-seq data were deposited in GEO database (GEO: GSE135278).

Apoptotic cell detection: CellEvent™ Caspase-3&7 Green Flow Cytometry Assay Kit (Life Technologies) was used to detect Caspase 3 and 7 activities inside the cells. Lung, spleen or tumor cells were incubated with CellEvent Caspase3&7 green detection reagent for 25 minutes at 37 degree as described in the manual.

Epigenetic screen: $CD8^+$ T cells from IFNγ-eYFP reporter mice (GREAT) were purified with the CD8a (Ly-2) MicroBeads (Miltenyi Biotech), and co-cultured with BMDC in presence of anti-CD3 (1 μg / ml) for 2.5 days, then compounds from Epigenetics Screening Library (Cayman chemical) were added into culture-system (10 μM each). Cells were harvested 24 hours later. YFP fluorescence and viability were analyzed by flow cytometer.

Intracellular staining, antibodies and flow cytometry: Cell suspensions were stained with indicated surface marker, staining was performed at 4 °C for 30 min. Cells were washed twice with FACS buffer (PBS, 2 mM EDTA, 2% FBS, 0.09% Sodium Azide), prior to fixation and permeabilization with either Perm Fix and Perm Wash (Biolegend, for cytokine staining) or the Foxp3 transcription factor staining buffer set (eBioscience, for KI-67 and AceH3 staining) in the dark. Cells were washed twice with perm wash (biolegend or eBioscience), stained with Abs for at least 30 min at RT and then washed twice with perm wash before flow cytometry acquisition. FACS Abs were primarily purchased from Biolegend, BD Biosciences or eBioscience. The clone number of those Abs as follows: CD8a (53-6.7), CD8β (YTS156.7.7), CD45(30-F11), CD90.1(OX-7), CD90.2(53-2.1), PD-1(29F.1A12), TIM-3(RMT3-23), CTLA4(UC10-4B9), CD103(2E7), CD69(H1.2F3), IFN-γ(XMG1.2), TNF-α(MP6-XT22), GzmB(GB11), MIP1-α(DNT3CC), MIP1 β(FL34Z3L),KI-67(SolA15), human CD8a(HIT8a), human PD1(EH12.2H7), human CD11a(HI111), human CD45RO(UCHL1).The dilution of surface staining Abs was 1:200 and dilution of intracellular staining Abs was 1:100. H2-D^b-$NP_{366-374}$ and H2-D^b-$PA_{224-233}$ tetramers were obtained from NIH tetramer facility. For prime-flow (eBioscience) staining, cells were stained with zombie dye (Biolegend) first then surface and intracellular staining were performed following instruction, then human or mouse RNA probes were hydrated and labeled with fluorescence dye. After Ab staining, cells were acquired through an 11-color Attune NXT system (Life Technologies). Data were then analyzed by FlowJo software (Treestar).

Antibody blockade *in vivo*: Anti-PD-L1 and control Abs were purchased from Bio-X-Cell. For systemic PD-L1 blockade in tumor model, WT B6 mice bearing B16-OVA melanoma received intraperitoneal injection of control or blocking Abs at the dose of 200 μg/ mouse for the first time at 5 days post tumor implantation, mice were then received intraperitoneal injection of Abs every 3 days with 50 μg/mouse thereafter. For measurement of *Bhlhe40* expression following intratumor PD-L1 blockade, α-PD-L1 injection was performed at the dose of 30 μg/ mouse at 6 days post tumor implantation, the blockade was applied every 3 days. For the depletion of circulating $CD8^+$ T cells, mice were received 50μg/ mouse anti-CD8a antibody at 21 d.p.i. For blocking $CD8^+$ T cells circulation, mice were received with

FTY720 (20μg/ mouse) daily since 21 d.p.i.. Peripheral $CD8^+$ T cells were checked in the PBMC one day before mouse sacrifice.

Transmission electron microscopy: $CD8^+$ T cells from *in vitro* culture, tumor implanted mice or influenza infected mice were isolated as indicated in the text. Cells were then fixed in Trump's Fixative, embedded and sliced for electron microscopy scanning. Quantitative analysis of mitochondrial damage was performed by blind review of two investigators on enlarged electron microscopy images (from n= 8-10 mice). Structurally abnormal mitochondria were defined operationally as those with loss of cristae, disarrayed cristae, decreased electron density of the matrix, loss of integrity of mitochondrial membrane and/or the formation of autophagosomes structures as reported before (Sohn et al., 2013; Wang et al., 2010).

Cellular therapy: For treatment at 6 d.p.t.i., B16-OVA cells ($5 \chi 10^5$) were implanted subcutaneously into C57BL/6 mice. On day 6 post implantation, tumor bearing mice with similar tumor size were divided into 4 groups randomly, and received with PBS, *in vitro* activated WT OTI cells (3 d.p.a. following *in vitro* activation, 1 million cells/mouse) or *in vitro* activated *Bhlhe40*$^{-/-}$ OTI cells (3 d.p.a. following *in vitro* activation, 1 million cells/ mouse) or *in vitro* activated *Bhlhe40*$^{-/-}$ OTI cells (3 d.p.a. following *in vitro* activation, 1 million cells/mouse) treated with Tubastatin A (10 μM, TA) (Selleckchem) and Sodium Acetate (20μM, Ac) (Sigma). Ac and TA were added to the culture at day 2 and 2.5 post activation respectively. Cells were washed with PBS before transferred into B16-OVA bearing mice at 6 d.p.t.i. After T cell transfer, tumor size was measured every two days. For cellular therapy of WT T cells into mice with large tumor burdens, WT OTI cells were activated *in vitro* (3 d.p.a.) and treated with TA and Ac as above. Cells (1 million cells/ mouse) were washed with PBS before transferred into B16-OVA bearing mice at 10 or 12 d.p.t.i. as indicated in the text.

Checkpoint blockade and chemical therapy: 11 days after B16-OVA tumor implantation, mice were intratumorally injected with anti-PD-L1 (30 μg / mouse) every 3 days. Sodium acetate (100 nmol/mouse) plus Tubastatin A (60 μg / mouse) were directly injected intratumorally daily from 11 days post B16-OVA tumor or 15 days post MC38 tumor implantation. Tumor size was calculated as length χ width. Mice with tumor size larger than 400 mm^2 or ulcerative were euthanized and considered as mortality caused by tumor.

Nanostring analysis: Total RNA from sorted T cell populations (n=4-12 mice/group) was extracted with mini RNA-easy Kit (Qiagen). Equal amount of total RNA from different cells was used for the assay. Hybridization reaction was established by following the instruction of manufacture. Aliquots of Reporter Codeset and Capture probeset were thawed at room temperature. Then a master of mix was created by adding 70ul of hybridization buffer to the tube containing the reporter codeset. 8 μl of this master mix was added to each of tubes for different samples, 5 μl (50 ng) of total RNA sample was added into each tube. Then 2 μl of well mixed Capture probeset was added to each tube and placed in the preheated 65°C thermal cycler. All the sample mixes were incubated for 16 hours at 65°C for completion of hybridization. The samples were then loaded into the sample hole in the cartridge and loaded

into the NanoString nCounter SPRINT Profiler machine (NanoString). When corresponding RLF running is finished, the raw data was downloaded and analyzed with Nanostring software nSolver 3.0 (Nanostring). mRNA counts were processed to account for hybridization efficiency, background noise, and sample content, and were normalized using the geometric mean of housekeeping genes. Fold changes were calculated comparing the experimental group to their appropriate controls.

Stable isotope tracer analysis (SITA) analysis: WT or *Bhlhe40*$^{-/-}$ CD8^{+} T cells were activated in vitro for 3.5 days, then the culture medium was replaced with medium which contains [^{13}C-3]-pyruvate or [^{13}C-5]-glutamine, incubating overnight. Cells were washed twice with PBS following removing culture medium, then cells were suspended with PBS/ Methanol (1:1) for GC/MS analysis.

Metabolite analysis: For qualitative large-scale profiling of metabolites, (5 million) WT or *Bhlhe40*$^{-/-}$ CD8^{+} T cells were activated *in vitro* for 4 days, Cells pellet was lyzed in 1xPBS and was deproteinized with acetonitrile:methanol (1:1 ratio). The supernatants were dried down using a stream of nitrogen gas for analysis on a Quadrupole Time-of-Flight Mass Spectrometer (Agilent Technologies 6550 Q-TOF) coupled with an Ultra High Pressure Liquid Chromatograph (1290 Infinity UHPLC Agilent Technologies).

Profiling data was acquired under both positive and negative electrospray ionization conditions over a mass range m/z of 100 – 1700 at a resolution of 10,000 (separate runs) in scan mode. Metabolite separation was achieved using two columns of differing polarity, a hydrophilic interaction column (HILIC, ethylene-bridged hybrid 2.1 × 150 mm, 1.7 mm; Waters) and a reversed-phase C18 column (high-strength silica 2.1 × 150 mm, 1.8 mm; Waters).

For TCA-analytes testing, *in vitro* activated CD8^{+} T cell pellets (2 million) was lyzed acidified 1X PBS after spiking in internal solution containing U-13C labeled analytes. The proteins were removed by methanol and acetonitrile. After drying, the sample was derivatized with ethoxime and then with MtBSTFA $^{+}$ 1% tBDMCS (N-Methyl-N-(t-Butyldimethylsilyl)-Trifluoroacetamide $^{+}$ 1% t-Butyldimethylchlorosilane) before it was analyzed on an Agilent 5975C GC/MS (gas chromatography/mass spectrometry) under electron impact and single ion monitoring conditions. Concentrations of lactic acid (m/z 261.2), fummaric acid (m/z 287.1), succinic acid (m/z 289.1), oxaloacetic acid (m/z 346.2), ketoglutaric acid (m/z 360.2), malic acid (m/z 419.3), aspartic acid (m/z 418.2), 2-hydroxyglutaratic acid (m/z 433.2), cis aconitic acid (m/z459.3), citric acid (m/z 591.4), and isocitric acid (m/z 591.4), glutamic acid (m/z 432.4) were measured against a 7-point calibration curves that underwent the same derivatization.

Statistical Analysis: Statistical analysis was done using GraphPad Prism 7.0 (GraphPad Software) and presented as means ± SEM. Unpaired or paired Student *t* tests and one-way or two-way ANOVA analysis were used in data analysis. A p value <0.05 was considered statistically significant. * $p < 0.05$. ** $p < 0.01$, *** $p < 0.001$,**** $p < 0.0001$.

Supplementary Material

Refer to Web version on PubMed Central for supplementary material.

ACKNOWLEDGEMENT

We thank NIH tetramer core for tetramers and H. Zhang for scRNA-seq analysis. This study was funded by the US National Institutes of Health RO1s AI112844, AG047156 and HL126647 (J.S.), R01s HL056470 and HL126451 (P.K.S.), R01 AI057459 (M.H.K.), R01 CA217987 (J.C.R.), R01s AI113118 and AI132653 (B.T.E.). K.E.B. receives funding from the Merck-Cancer Research Institute Irvington Post-doctoral fellowship. P.J.S. is supported by Else Kroener Fresenius Stiftung.

References:

Anderson KG, Mayer-Barber K, Sung H, Beura L, James BR, Taylor JJ, Qunaj L, Griffith TS, Vezys V, Barber DL, and Masopust D (2014). Intravascular staining for discrimination of vascular and tissue leukocytes. Nat Protoc 9, 209–222. [PubMed: 24385150]

Ariotti S, Hogenbirk MA, Dijkgraaf FE, Visser LL, Hoekstra ME, Song JY, Jacobs H, Haanen JB, and Schumacher TN (2014). T cell memory. Skin-resident memory CD8(+) T cells trigger a state of tissue-wide pathogen alert. Science 346, 101–105. [PubMed: 25278612]

Azizi E, Carr AJ, Plitas G, Cornish AE, Konopacki C, Prabhakaran S, Nainys J, Wu K, Kiseliovas V, Setty M, et al. (2018). Single-Cell Map of Diverse Immune Phenotypes in the Breast Tumor Microenvironment. Cell 174, 1293–1308 e1236. [PubMed: 29961579]

Balmer ML, Ma EH, Bantug GR, Grahlert J, Pfister S, Glatter T, Jauch A, Dimeloe S, Slack E, Dehio P, et al. (2016). Memory CD8(+) T Cells Require Increased Concentrations of Acetate Induced by Stress for Optimal Function. Immunity 44, 1312–1324. [PubMed: 27212436]

Bantug GR, Fischer M, Grahlert J, Balmer ML, Unterstab G, Develioglu L, Steiner R, Zhang L, Costa ASH, Gubser PM, et al. (2018). Mitochondria-Endoplasmic Reticulum Contact Sites Function as Immunometabolic Hubs that Orchestrate the Rapid Recall Response of Memory CD8(+) T Cells. Immunity 48, 542–555 e546. [PubMed: 29523440]

Borges da Silva H, Beura LK, Wang H, Hanse EA, Gore R, Scott MC, Walsh DA, Block KE, Fonseca R, Yan Y, et al. (2018). The purinergic receptor P2RX7 directs metabolic fitness of long-lived memory CD8(+) T cells. Nature 559, 264–268. [PubMed: 29973721]

Buck MD, O'Sullivan D, Klein Geltink RI, Curtis JD, Chang CH, Sanin DE, Qiu J, Kretz O, Braas D, van der Windt GJ, et al. (2016). Mitochondrial Dynamics Controls T Cell Fate through Metabolic Programming. Cell 166, 63–76. [PubMed: 27293185]

Chang CH, Qiu J, O'Sullivan D, Buck MD, Noguchi T, Curtis JD, Chen Q, Gindin M, Gubin MM, van der Windt GJ, et al. (2015). Metabolic Competition in the Tumor Microenvironment Is a Driver of Cancer Progression. Cell 162, 1229–1241. [PubMed: 26321679]

Colgan SP, Campbell EL, and Kominsky DJ (2016). Hypoxia and Mucosal Inflammation. Annu Rev Pathol 11, 77–100. [PubMed: 27193451]

Dong H, Strome SE, Salomao DR, Tamura H, Hirano F, Flies DB, Roche PC, Lu J, Zhu G, Tamada K, et al. (2002). Tumor-associated B7-H1 promotes T-cell apoptosis: a potential mechanism of immune evasion. Nat Med 8, 793–800. [PubMed: 12091876]

Dronca RS, Liu X, Harrington SM, Chen L, Cao S, Kottschade LA, McWilliams RR, Block MS, Nevala WK, Thompson MA, et al. (2016). T cell Bim levels reflect responses to anti-PD-1 cancer therapy. JCI Insight 1.

Ganesan AP, Clarke J, Wood O, Garrido-Martin EM, Chee SJ, Mellows T, Samaniego-Castruita D, Singh D, Seumois G, Alzetani A, et al. (2017). Tissue-resident memory features are linked to the magnitude of cytotoxic T cell responses in human lung cancer. Nat Immunol 18, 940–950. [PubMed: 28628092]

Gebhardt T, Wakim LM, Eidsmo L, Reading PC, Heath WR, and Carbone FR (2009). Memory T cells in nonlymphoid tissue that provide enhanced local immunity during infection with herpes simplex virus. Nat Immunol 10, 524–530. [PubMed: 19305395]

Ghoneim HE, Fan Y, Moustaki A, Abdelsamed HA, Dash P, Dogra P, Carter R, Awad W,Neale G, Thomas PG, and Youngblood B (2017). De Novo Epigenetic Programs Inhibit PD-1 Blockade-Mediated T Cell Rejuvenation. Cell 170, 142–157 e119. [PubMed: 28648661]

Greene CS, Krishnan A, Wong AK, Ricciotti E, Zelaya RA, Himmelstein DS, Zhang R, Hartmann BM, Zaslavsky E, Sealfon SC, et al. (2015). Understanding multicellular function and disease with human tissue-specific networks. Nat Genet 47, 569–576. [PubMed: 25915600]

Guo X, Zhang Y, Zheng L, Zheng C, Song J, Zhang Q, Kang B, Liu Z, Jin L, Xing R, et al. (2018). Global characterization of T cells in non-small-cell lung cancer by single-cell sequencing. Nat Med 24, 978–985. [PubMed: 29942094]

Hamieh M, Dobrin A, Cabriolu A, van der Stegen SJC, Giavridis T, Mansilla-Soto J, Eyquem J, Zhao Z, Whitlock BM, Miele MM, et al. (2019). CAR T cell trogocytosis and cooperative killing regulate tumour antigen escape. Nature 568, 112–116. [PubMed: 30918399]

Henning AN, Roychoudhuri R, and Restifo NP (2018). Epigenetic control of CD8(+) T cell differentiation. Nat Rev Immunol 18, 340–356. [PubMed: 29379213]

Hombrink P, Helbig C, Backer RA, Piet B, Oja AE, Stark R, Brasser G, Jongejan A, Jonkers RE, Nota B, et al. (2016). Programs for the persistence, vigilance and control of human CD8(+) lung-resident memory T cells. Nat Immunol 17, 1467–1478. [PubMed: 27776108]

Hu G, and Chen J (2013). A genome-wide regulatory network identifies key transcription factors for memory CD8(+) T-cell development. Nat Commun 4, 2830. [PubMed: 24335726]

Huynh JP, Lin CC, Kimmey JM, Jarjour NN, Schwarzkopf EA, Bradstreet TR, Shchukina I, Shpynov O, Weaver CT, Taneja R, et al. (2018). Bhlhe40 is an essential repressor of IL-10 during Mycobacterium tuberculosis infection. J Exp Med 215, 1823–1838. [PubMed: 29773644]

Iborra S, Martinez-Lopez M, Khouili SC, Enamorado M, Cueto FJ, Conde-Garrosa R, Del Fresno C, and Sancho D (2016). Optimal Generation of Tissue-Resident but Not Circulating Memory T Cells during Viral Infection Requires Crosspriming by DNGR-1(+) Dendritic Cells. Immunity 45, 847–860. [PubMed: 27692611]

Jiang X, Clark RA, Liu L, Wagers AJ, Fuhlbrigge RC, and Kupper TS (2012). Skin infection generates non-migratory memory CD8+ T(RM) cells providing global skin immunity. Nature 483, 227–231. [PubMed: 22388819]

Kanda M, Yamanaka H, Kojo S, Usui Y, Honda H, Sotomaru Y, Harada M, Taniguchi M,Suzuki N, Atsumi T, et al. (2016). Transcriptional regulator Bhlhe40 works as a cofactor of T-bet in the regulation of IFN-gamma production in iNKT cells. Proc Natl Acad Sci U S A 113, E3394–3402. [PubMed: 27226296]

Kumar BV, Ma W, Miron M, Granot T, Guyer RS, Carpenter DJ, Senda T, Sun X, Ho SH, Lerner H, et al. (2017). Human Tissue-Resident Memory T Cells Are Defined by Core Transcriptional and Functional Signatures in Lymphoid and Mucosal Sites. Cell Rep 20, 2921–2934. [PubMed: 28930685]

Kurtulus S, Madi A, Escobar G, Klapholz M, Nyman J, Christian E, Pawlak M, Dionne D, Xia J, Rozenblatt-Rosen O, et al. (2019). Checkpoint Blockade Immunotherapy Induces Dynamic Changes in PD-1(−)CD8(+) Tumor-Infiltrating T Cells. Immunity 50, 181–194 e186. [PubMed: 30635236]

Laidlaw BJ, Zhang N, Marshall HD, Staron MM, Guan T, Hu Y, Cauley LS, Craft J, and Kaech SM (2014). CD4+ T cell help guides formation of CD103+ lung-resident memory CD8+ T cells during influenza viral infection. Immunity 41, 633–645. [PubMed: 25308332]

Li H, van der Leun AM, Yofe I, Lubling Y, Gelbard-Solodkin D, van Akkooi ACJ, van den Braber M, Rozeman EA, Haanen J, Blank CU, et al. (2019). Dysfunctional CD8 T Cells Form a Proliferative, Dynamically Regulated Compartment within Human Melanoma. Cell 176, 775–789 e718. [PubMed: 30595452]

Lin CC, Bradstreet TR, Schwarzkopf EA, Jarjour NN, Chou C, Archambault AS, Sim J, Zinselmeyer BH, Carrero JA, Wu GF, et al. (2016). IL-1-induced Bhlhe40 identifies pathogenic T helper cells in a model of autoimmune neuroinflammation. J Exp Med 213, 251–271. [PubMed: 26834156]

Lin CC, Bradstreet TR, Schwarzkopf EA, Sim J, Carrero JA, Chou C, Cook LE, Egawa T, Taneja R, Murphy TL, et al. (2014). Bhlhe40 controls cytokine production by T cells and is essential for pathogenicity in autoimmune neuroinflammation. Nat Commun 5, 3551. [PubMed: 24699451]

M L, P PV, T K, M P, E S, J P, K VW, C L., F C, S D, et al. (2016). Essential role of HDAC6 in the regulation of PD-L1 in melanoma. Mol Oncol 10, 735–750. [PubMed: 26775640]

Ma W, Shi X, Lu S, Wu L, and Wang Y (2013). Hypoxia-induced overexpression of DEC1 is regulated by HIF-1alpha in hepatocellular carcinoma. Oncol Rep 30, 2957–2962. [PubMed: 24100543]

Mackay LK, Minnich M, Kragten NA, Liao Y, Nota B, Seillet C, Zaid A, Man K, Preston S, Freestone D, et al. (2016). Hobit and Blimp1 instruct a universal transcriptional program of tissue residency in lymphocytes. Science 352, 459–463. [PubMed: 27102484]

Mehta MM, Weinberg SE, and Chandel NS (2017). Mitochondrial control of immunity: beyond ATP. Nat Rev Immunol 17, 608–620. [PubMed: 28669986]

Milner JJ, Toma C, Yu B, Zhang K, Omilusik K, Phan AT, Wang D, Getzler AJ, Nguyen T, Crotty S, et al. (2017). Runx3 programs CD8(+) T cell residency in non-lymphoid tissues and tumours. Nature 552, 253–257. [PubMed: 29211713]

Nunez-Andrade N, Iborra S, Trullo A, Moreno-Gonzalo O, Calvo E, Catalan E, Menasche G, Sancho D, Vazquez J, Yao TP, et al. (2016). HDAC6 regulates the dynamics of lytic granules in cytotoxic T lymphocytes. J Cell Sci 129, 1305–1311. [PubMed: 26869226]

Pan Y, Tian T, Park CO, Lofftus SY, Mei S, Liu X, Luo C, O'Malley JT, Gehad A, Teague JE, et al. (2017). Survival of tissue-resident memory T cells requires exogenous lipid uptake and metabolism. Nature 543, 252–256. [PubMed: 28219080]

Pauken KE, Sammons MA, Odorizzi PM, Manne S, Godec J, Khan O, Drake AM, Chen Z,Sen DR, Kurachi M, et al. (2016). Epigenetic stability of exhausted T cells limits durability of reinvigoration by PD-1 blockade. Science 354, 1160–1165. [PubMed: 27789795]

Pearce EL, Walsh MC, Cejas PJ, Harms GM, Shen H, Wang LS, Jones RG, and Choi Y (2009). Enhancing CD8 T-cell memory by modulating fatty acid metabolism. Nature 460, 103–107. [PubMed: 19494812]

Peng M, Yin N, Chhangawala S, Xu K, Leslie CS, and Li MO (2016). Aerobic glycolysis promotes T helper 1 cell differentiation through an epigenetic mechanism. Science 354, 481–484. [PubMed: 27708054]

Philip M, Fairchild L, Sun L, Horste EL, Camara S, Shakiba M, Scott AC, Viale A, Lauer P, Merghoub T, et al. (2017). Chromatin states define tumour-specific T cell dysfunction and reprogramming. Nature 545, 452–456. [PubMed: 28514453]

Poggio M, Hu T, Pai CC, Chu B, Belair CD, Chang A, Montabana E, Lang UE, Fu Q, Fong L, and Blelloch R (2019). Suppression of Exosomal PD-L1 Induces Systemic Anti-tumor Immunity and Memory. Cell 177, 414–427 e413. [PubMed: 30951669]

Precopio ML, Betts MR, Parrino J, Price DA, Gostick E, Ambrozak DR, Asher TE, Douek DC, Harari A, Pantaleo G, et al. (2007). Immunization with vaccinia virus induces polyfunctional and phenotypically distinctive CD8(+) T cell responses. J Exp Med 204, 1405–1416. [PubMed: 17535971]

Qiu J, Villa M, Sanin DE, Buck MD, O'Sullivan D, Ching R, Matsushita M, Grzes KM, Winkler F, Chang CH, et al. (2019). Acetate Promotes T Cell Effector Function during Glucose Restriction. Cell Rep 27, 2063–2074 e2065. [PubMed: 31091446]

Rabinovich GA, Gabrilovich D, and Sotomayor EM (2007). Immunosuppressive strategies that are mediated by tumor cells. Annu Rev Immunol 25, 267–296. [PubMed: 17134371]

Ribas A (2015). Adaptive Immune Resistance: How Cancer Protects from Immune Attack. Cancer Discov 5, 915–919. [PubMed: 26272491]

Sarkar S, Kalia V, Haining WN, Konieczny BT, Subramaniam S, and Ahmed R (2008). Functional and genomic profiling of effector CD8 T cell subsets with distinct memory fates. J Exp Med 205, 625–640. [PubMed: 18316415]

Savas P, Virassamy B, Ye C, Salim A, Mintoff CP, Caramia F, Salgado R, Byrne DJ, Teo ZL, Dushyanthen S, et al. (2018). Single-cell profiling of breast cancer T cells reveals a tissue-resident memory subset associated with improved prognosis. Nat Med 24, 986–993. [PubMed: 29942092]

Scharping NE, Menk AV, Moreci RS, Whetstone RD, Dadey RE, Watkins SC, Ferris RL, and Delgoffe GM (2016). The Tumor Microenvironment Represses T Cell Mitochondrial Biogenesis to Drive Intratumoral T Cell Metabolic Insufficiency and Dysfunction. Immunity 45, 374–388. [PubMed: 27496732]

Sen DR, Kaminski J, Barnitz RA, Kurachi M, Gerdemann U, Yates KB, Tsao HW, Godec J, LaFleur MW, Brown FD, et al. (2016). The epigenetic landscape of T cell exhaustion. Science 354, 1165–1169. [PubMed: 27789799]

Sena LA, Li S, Jairaman A, Prakriya M, Ezponda T, Hildeman DA, Wang CR, Schumacker PT, Licht JD, Perlman H, et al. (2013). Mitochondria are required for antigen-specific T cell activation through reactive oxygen species signaling. Immunity 38, 225–236. [PubMed: 23415911]

Sharma P, Hu-Lieskovan S, Wargo JA, and Ribas A (2017). Primary, Adaptive, and Acquired Resistance to Cancer Immunotherapy. Cell 168, 707–723. [PubMed: 28187290]

Siddiqui I, Schaeuble K, Chennupati V, Fuertes Marraco SA, Calderon-Copete S, Pais Ferreira D, Carmona SJ, Scarpellino L, Gfeller D, Pradervand S, et al. (2019). Intratumoral Tcf1(+)PD-1(+)CD8(+) T Cells with Stem-like Properties Promote Tumor Control in Response to Vaccination and Checkpoint Blockade Immunotherapy. Immunity 50, 195–211 e110. [PubMed: 30635237]

Singer M, Wang C, Cong L, Marjanovic ND, Kowalczyk MS, Zhang H, Nyman J, Sakuishi K, Kurtulus S, Gennert D, et al. (2016). A Distinct Gene Module for Dysfunction Uncoupled from Activation in Tumor-Infiltrating T Cells. Cell 166, 1500–1511 e1509. [PubMed: 27610572]

Skon CN, Lee JY, Anderson KG, Masopust D, Hogquist KA, and Jameson SC (2013). Transcriptional downregulation of S1pr1 is required for the establishment of resident memory CD8+ T cells. Nat Immunol 14, 1285–1293. [PubMed: 24162775]

Sohn YS, Tamir S, Song L, Michaeli D, Matouk I, Conlan AR, Harir Y, Holt SH, Shulaev V, Paddock ML, et al. (2013). NAF-1 and mitoNEET are central to human breast cancer proliferation by maintaining mitochondrial homeostasis and promoting tumor growth. Proc Natl Acad Sci U S A 110, 14676–14681. [PubMed: 23959881]

Sun H, Lu B, Li RQ, Flavell RA, and Taneja R (2001). Defective T cell activation and autoimmune disorder in Stra13-deficient mice. Nat Immunol 2, 1040–1047. [PubMed: 11668339]

Sun J, Dodd H, Moser EK, Sharma R, and Braciale TJ (2011). CD4+ T cell help and innate-derived IL-27 induce Blimp-1-dependent IL-10 production by antiviral CTLs. Nat Immunol 12, 327–334. [PubMed: 21297642]

Sun J, Madan R, Karp CL, and Braciale TJ (2009). Effector T cells control lung inflammation during acute influenza virus infection by producing IL-10. Nat Med 15, 277–284. [PubMed: 19234462]

Sun J, and Pearce EJ (2007). Suppression of early IL-4 production underlies the failure of CD4 T cells activated by TLR-stimulated dendritic cells to differentiate into Th2 cells. J Immunol 178, 1635–1644. [PubMed: 17237413]

Tang H, Liang Y, Anders RA, Taube JM, Qiu X, Mulgaonkar A, Liu X, Harrington SM, Guo J, Xin Y, et al. (2018). PD-L1 on host cells is essential for PD-L1 blockade-mediated tumor regression. J Clin Invest 128, 580–588. [PubMed: 29337303]

Thomas PG, Keating R, Hulse-Post DJ, and Doherty PC (2006). Cell-mediated protection in influenza infection. Emerg Infect Dis 12, 48–54. [PubMed: 16494717]

Topalian SL, Hodi FS, Brahmer JR, Gettinger SN, Smith DC, McDermott DF, Powderly JD, Carvajal RD, Sosman JA, Atkins MB, et al. (2012). Safety, activity, and immune correlates of anti-PD-1 antibody in cancer. N Engl J Med 366, 2443–2454. [PubMed: 22658127]

Trompette A, Gollwitzer ES, Pattaroni C, Lopez-Mejia IC, Riva E, Pernot J, Ubags N, Fajas L, Nicod LP, and Marsland BJ (2018). Dietary Fiber Confers Protection against Flu by Shaping Ly6c(−) Patrolling Monocyte Hematopoiesis and CD8(+) T Cell Metabolism. Immunity 48, 992–1005 e1008. [PubMed: 29768180]

Wang Q, Frolova AI, Purcell S, Adastra K, Schoeller E, Chi MM, Schedl T, and Moley KH (2010). Mitochondrial dysfunction and apoptosis in cumulus cells of type I diabetic mice. PLoS One 5, e15901. [PubMed: 21209947]

Wellen KE, Hatzivassiliou G, Sachdeva UM, Bui TV, Cross JR, and Thompson CB (2009). ATP-citrate lyase links cellular metabolism to histone acetylation. Science 324, 1076–1080. [PubMed: 19461003]

Yao S, Buzo BF, Pham D, Jiang L, Taparowsky EJ, Kaplan MH, and Sun J (2013). Interferon regulatory factor 4 sustains CD8(+) T cell expansion and effector differentiation. Immunity 39, 833–845. [PubMed: 24211184]

Yao S, Jiang L, Moser EK, Jewett LB, Wright J, Du J, Zhou B, Davis SD, Krupp NL, Braciale TJ, and Sun J (2015). Control of pathogenic effector T-cell activities in situ by PD-L1 expression on respiratory inflammatory dendritic cells during respiratory syncytial virus infection. Mucosal Immunol 8, 746–759. [PubMed: 25465101]

Yu F, Sharma S, Jankovic D, Gurram RK, Su P, Hu G, Li R, Rieder S, Zhao K, Sun B, and Zhu J (2018). The transcription factor Bhlhe40 is a switch of inflammatory versus antiinflammatory Th1 cell fate determination. J Exp Med 215, 1813–1821. [PubMed: 29773643]

Yuan J, Gnjatic S, Li H, Powel S, Gallardo HF, Ritter E, Ku GY, Jungbluth AA, Segal NH, Rasalan TS, et al. (2008). CTLA-4 blockade enhances polyfunctional NY-ESO-1 specific T cell responses in metastatic melanoma patients with clinical benefit. Proc Natl Acad Sci U S A 105, 20410–20415. [PubMed: 19074257]

Zhang L, Yu X, Zheng L, Zhang Y, Li Y, Fang Q, Gao R, Kang B, Zhang Q, Huang JY, et al. (2018). Lineage tracking reveals dynamic relationships of T cells in colorectal cancer. Nature 564, 268–272. [PubMed: 30479382]

Zhang Y, Kurupati R, Liu L, Zhou XY, Zhang G, Hudaihed A, Filisio F, Giles-Davis W, Xu X, Karakousis GC, et al. (2017). Enhancing CD8(+) T Cell Fatty Acid Catabolism within a Metabolically Challenging Tumor Microenvironment Increases the Efficacy of Melanoma Immunotherapy. Cancer Cell 32, 377–391 e379. [PubMed: 28898698]

Zhao E, Maj T, Kryczek I, Li W, Wu K, Zhao L, Wei S, Crespo J, Wan S, Vatan L, et al. (2016a). Cancer mediates effector T cell dysfunction by targeting microRNAs and EZH2 via glycolysis restriction. Nat Immunol 17, 95–103. [PubMed: 26523864]

Zhao S, Torres A, Henry RA, Trefely S, Wallace M, Lee JV, Carrer A, Sengupta A, Campbell SL, Kuo YM, et al. (2016b). ATP-Citrate Lyase Controls a Glucose-to-Acetate Metabolic Switch. Cell Rep 17, 1037–1052. [PubMed: 27760311]

Zheng C, Zheng L, Yoo JK, Guo H, Zhang Y, Guo X, Kang B, Hu R, Huang JY, Zhang Q, et al. (2017). Landscape of Infiltrating T Cells in Liver Cancer Revealed by Single-Cell Sequencing. Cell 169, 1342–1356 e1316. [PubMed: 28622514]

Highlights

- Bhlhe40 is required for Trm cell and TIL fitness and function.
- Bhlhe40 is critical for TIL reinvigoration following anti-PD-L1 blockade.
- Bhlhe40 programs Trm cell and TIL mitochondrial metabolism and active chromatin state.
- Epigenetic targeting Trm cell and TIL functional program promotes tumor control.

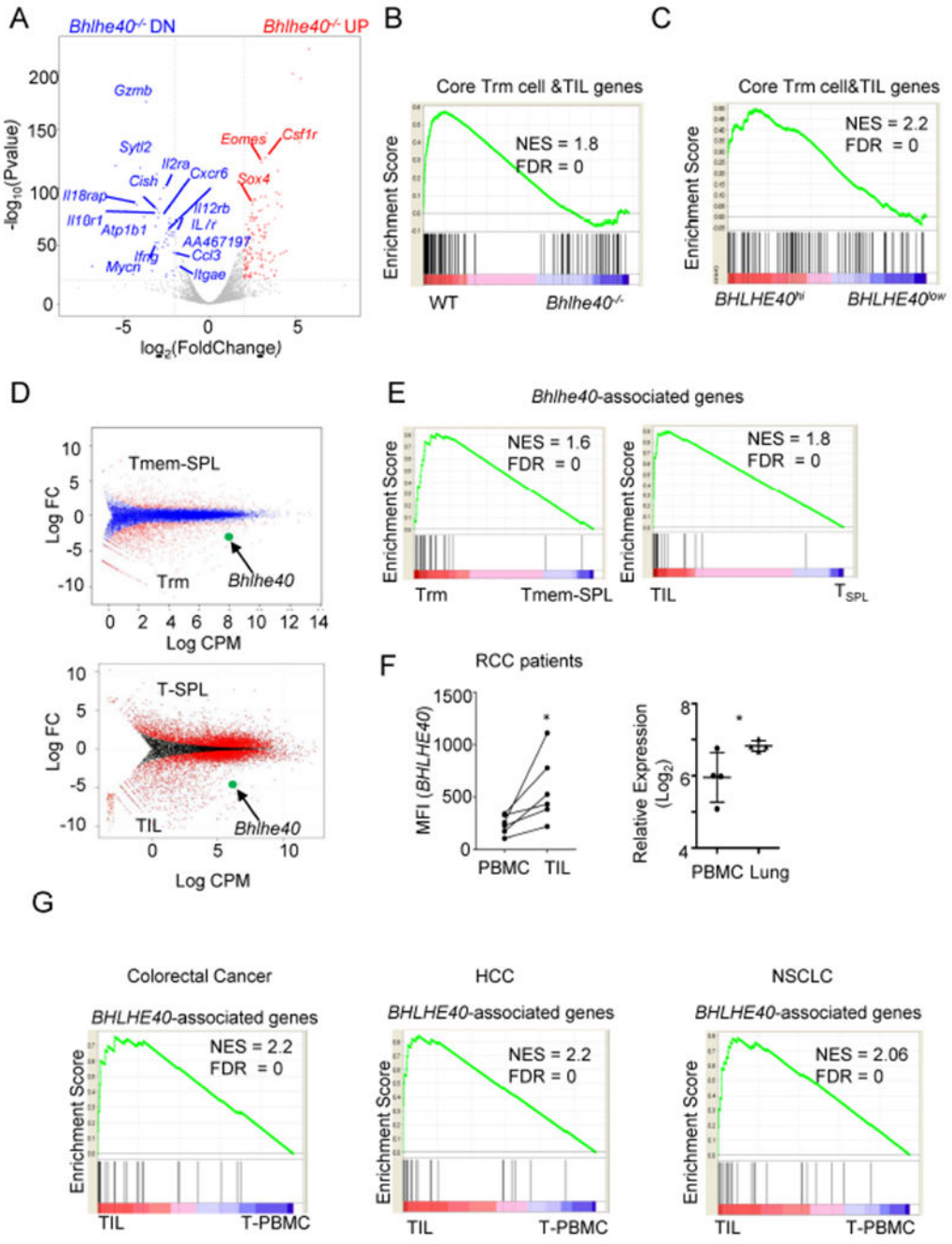

Figure 1. Increased *Bhlhe40* expression in tissue-resident CD8$^+$ T cells

(A) RNA-seq analysis of differentially expressed genes in activated WT vs. *Bhlhe40*$^{-/-}$ CD8$^+$ T cells (4 days post activation, d.p.a.).

(B) GSEA of the core tissue-residency signature genes of Trm cells and TILs in WT or *Bhlhe40*$^{-/-}$ CD8$^+$ T cells.

(C) GSEA of the core tissue-residency signature genes of Trm cells and TILs in *BHLHE40*^{hi} or *BHLHE40*^{low} TILs from colorectal cancer patients.

(D) RNA-seq analysis of Tmem-SPL vs. lung Trm cells post PR8-OVA infection (42 d.p.i.), or TILs vs. splenic $CD8^+$ T cells (T-SPL) post B16-OVA transplantation (12 d.p.t.i.).
(E) GSEA of *Bhlhe40*-associated gene set in Trm cells vs. Tmem-SPL cells, or TILs vs. T-SPL.
(F) Left, MFI of *BHLHE40* in tumor-reactive PBMC $CD8^+$ T cells or TILs from RCC patients (n=6); right, *BHLHE40* expression in human lung $CD8^+$ Trm cells or PBMC Tmem cells.
(G) GSEA of *BHLHE40*-associated gene set in TILs or PBMC $CD8^+$ T cells from colorectal cancer, liver cancer (HCC) and lung cancer (NSCLC) patients.
*$P \leq 0.05$ (Student's t-test). See also Figure S1.

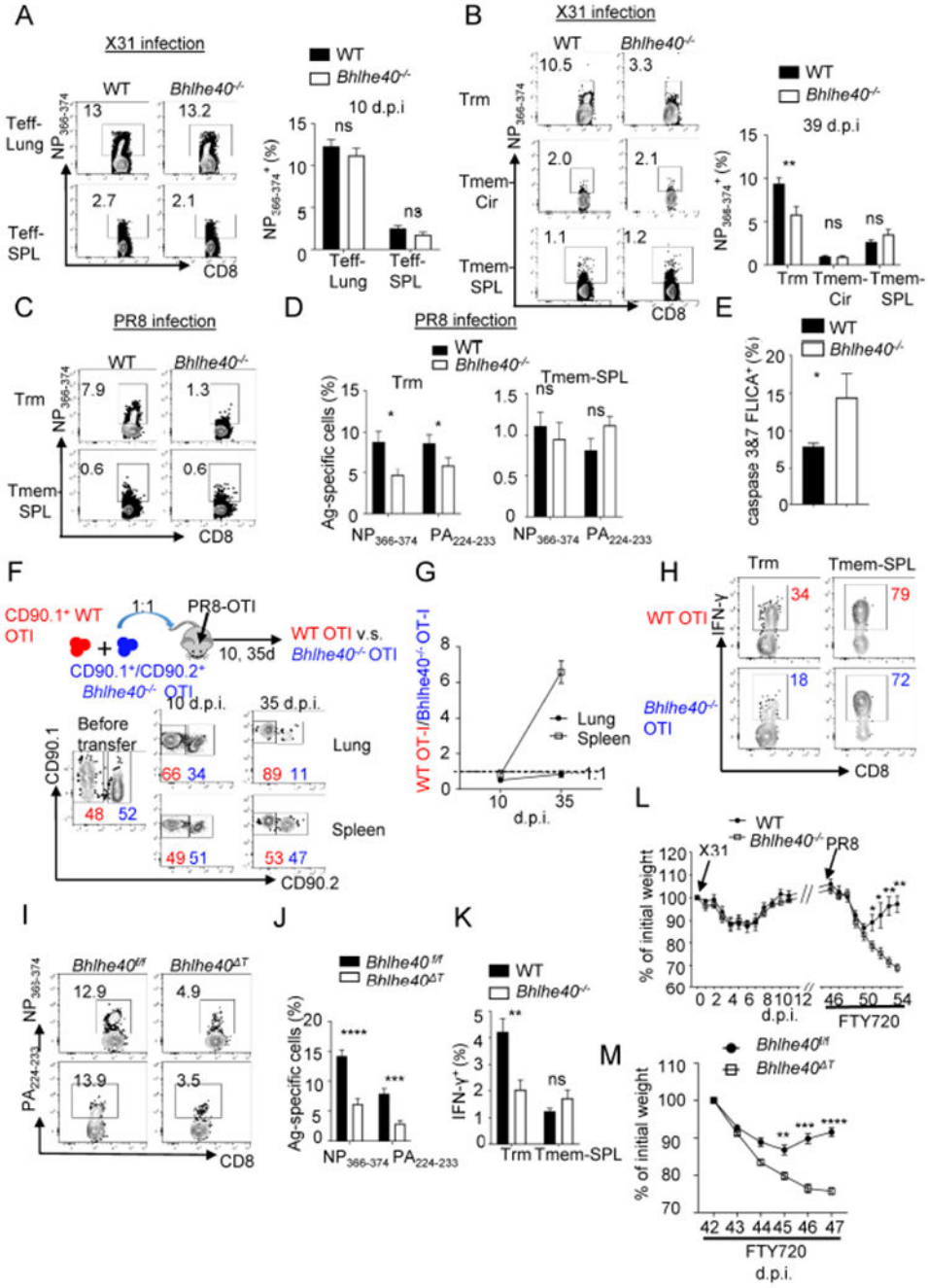

Figure 2. Bhlhe40 maintains function and survival of Trm cells

(A) % $NP_{366\text{-}374}^{+}$ Teff-Lung or Teff-SPL of WT or *Bhlh40*$^{-/-}$ mice following X31 infection at 10 d.p.i. (n=10, 2 experiments).

(B) % $NP_{366\text{-}374}^{+}$ Trm, lung circulating T memory (Tmem-Cir) or Tmem-SPL cells of WT or *Bhlh40*$^{-/-}$ mice following X31 infection at 39 d.p.i. (n=12-14, 3 experiments).

(C) and (D), % $NP_{366\text{-}374}^{+}$ and $PA_{224\text{-}233}^{+}$ Trm or Tmem-SPL cells from WT or *Bhlh40*$^{-/-}$ mice at 42 d.p. PR8 infection (n=11, 2 experiments).

(E) % apoptotic (Caspase 3&7 FLICA$^+$) $NP_{366-374}{}^+$ Trm cells at 42 d.p. PR8 infection (n= 5).

(F-H) WT and *Bhlhe40*$^{-/-}$ OTI cells were 1:1 mixed and transferred into recipient mice infected with PR8-OVA (n=12, 2 experiments). Representative plots (F) and ratio (G) of WT to *Bhlhe40*$^{-/-}$ OTI cells in the lung and spleen were evaluated at 10 and 35 d.p.i. (H) %IFN-γ^+ OTI cell after *ex vivo* peptide stimulation.

(I, J) Representative plots (I) and % (J) $NP_{366-374}{}^+$ or $PA_{224-233}{}^+$ Trm cells in *Bhlhe40*$^{f/f}$ or *Bhlhe40*$^{\Delta T}$ mice at 42 d.p. PR8 infection (n=8-9, 2 experiments).

(K) % IFN-γ^+ Trm or Tmem-SPL cells at 42 d.p. PR8 infection (n=8, 2 experiments).

(L) WT or *Bhlh40*$^{-/-}$ mice were infected with X31 and re-challenged with PR8 in the presence of FTY-720 at 45 d.p.i. % original weight was determined (n=3-4).

(M) *Bhlhe40*$^{f/f}$ or *Bhlhe40*$^{\Delta T}$ mice were infected with PR8 and re-challenged with X31 in the presence of FTY-720 at 42 d.p.i. % body weight before rechallenge was determined (n=5-7).

Representative data from 2 or 3 experiments except those data from pooled experiments. *$P \leq 0.05$, **$P \leq 0.01$, ***$P \leq 0.001$, ****$p < 0.0001$ (Student's t-test). See also Figure S2.

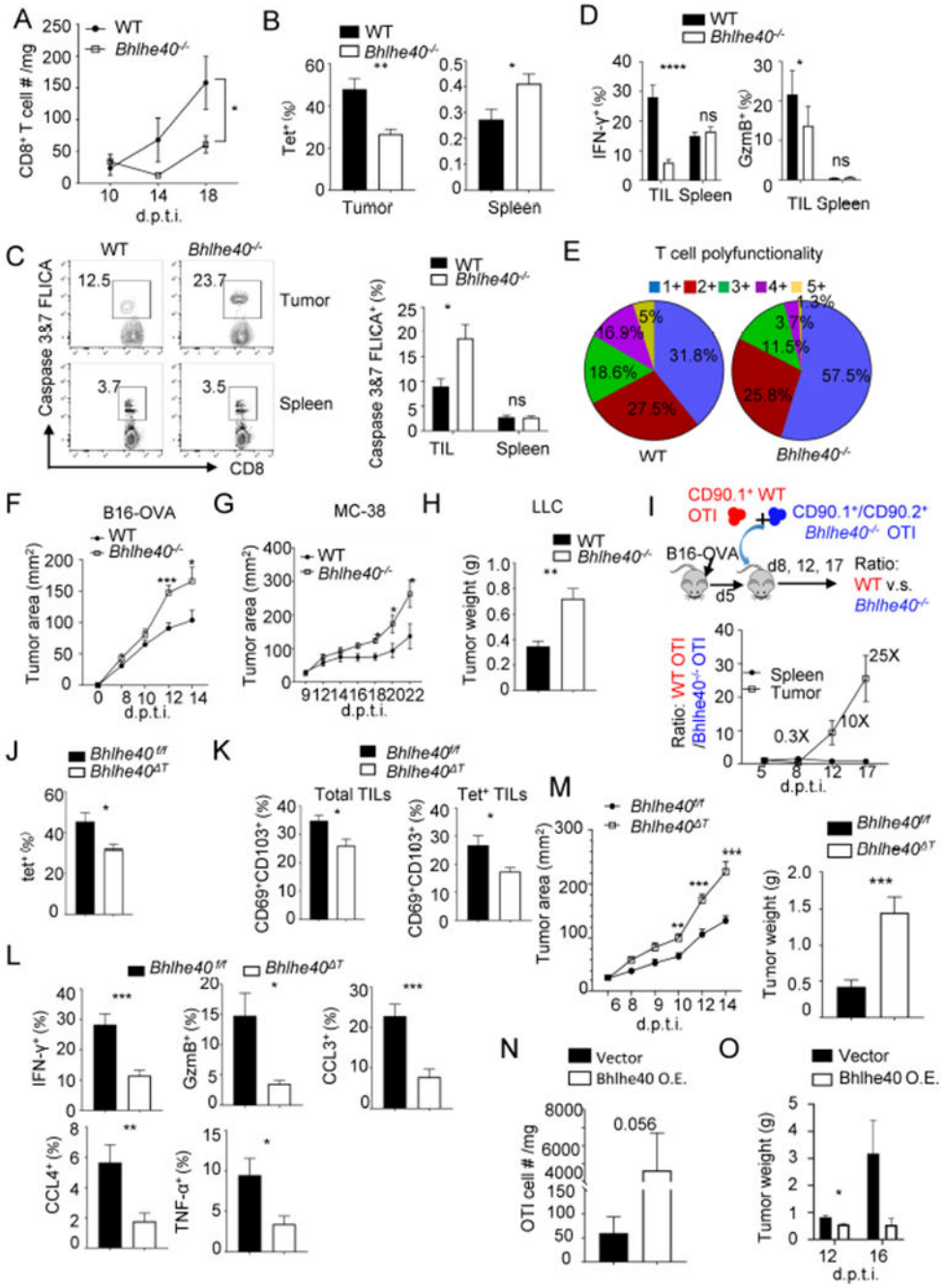

Figure 3. Bhlhe40 governs TIL responses and functionality

(A) TIL density ($CD8^+$ T cell #/mg tumor tissue) in B16-OVA tumor bearing WT or *Bhlhe40*$^{-/-}$ mice (n=3).

(B) % $OVA_{257\text{-}264}{}^+$ $CD8^+$ T cells in tumor or spleen (n=4-9, 2 experiments).

(C) Representative plots and % apoptotic (Caspase3&7 $FLICA^+$) $CD8^+$ T cells from tumor or spleen (n=7, 2 experiments).

(D) % IFN-γ^+ or $GzmB^+$ $CD8^+$ T cells from tumor or spleen of WT or *Bhlhe40*$^{-/-}$ mice (14 d.p.t.i.) (n=10, 2 experiments).

(E) The production of IFN-γ, TNF-α, GzmB, CCL3 and CCL4 by TILs (14 d.p.t.i.) were measured following *ex vivo* stimulation. After Boolean gating, individual populations were grouped based on the total number of effector molecules producing cells (n= 4-6).
(F-H) Indicated tumor growth curves (F (n=15-16, 4 experiments) and G (n=4)) or tumor weight (H) (n=4-5) in WT or *Bhlhe40*$^{-/-}$ mice.
(I) WT and *Bhlhe40*$^{-/-}$ OTI cells were 1:1 mixed and transferred into B16-OVA bearing mice. Ratio of WT to *Bhlhe40*$^{-/-}$ OTI cells was evaluated (n=8-9, 2 experiments).
(J-M) *Bhlhe40*$^{f/f}$ or *Bhlhe40*$^{\Delta T}$ mice were transplanted with B16-OVA. (J) % $OVA_{257\text{-}264}{}^{+}$ TILs at 14 d.p.t.i (n=5). (K) % $CD69^{+}CD103^{+}$ TILs at 14 d.p.t.i. in bulk or OVA specific TILs (n=5). (L) Cytokine and effector molecule production by TILs (n=8, 2 experiments). (M) B16-OVA growth curves (left) (n=14, 3 experiments) and tumor weight (right) (n=10, 2 experiments).
(N, O) B16-OVA bearing WT mice received OTI cells transduced with control (Vector) or Bhlhe40-expressing retrovirus (Bhlhe40 O.E.) at 5 d.p.t.i. (N) Cell counts of transferred cells inside tumor at 12 d.p.t.i. (O) Tumor weight (n=4-5).
Representative data from 2 to 4 experiments except those data from pooled experiments. $*P \leq 0.05$,$**P \leq 0.01$, $***P \leq 0.001$ (Student's t-test and Two-way ANOVA). See also Figure S3.

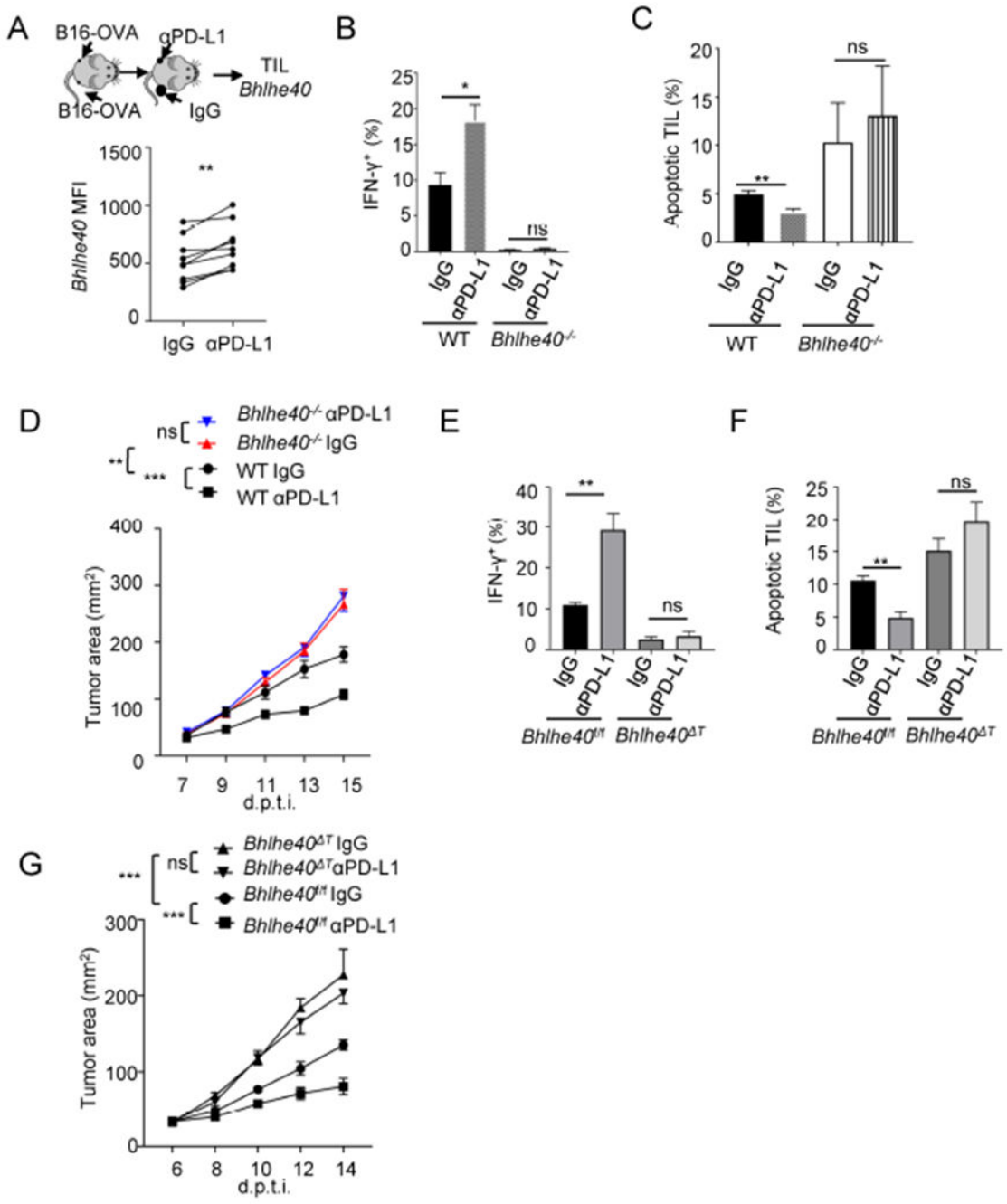

Figure 4. Bhlhe40 is required for T cell reinvigoration following PD-L1 blockade

(A) B16-OVA were implanted into both sides of flank following with intratumor injection of α-PD-L1 or control IgG to one side. MFI of *Bhlhe40* from TILs at 14 d.p.t.i. (n=9, 2 experiments).

(B-D) WT or *Bhlhe40*$^{-/-}$ B16-OVA bearing mice received control IgG or α-PD-L1 from 5 d.p.t.i. % IFN-γ^{+} TILs (B) or % apoptotic TILs (C) from indicated groups at 15 d.p.t.i. (n=9, 2 experiments). (D) Tumor growth curve (n=13-15, 3 experiments).

(E-G) *Bhlhe40*$^{f/f}$ or *Bhlhe40*$^{\Delta T}$ B16-OVA bearing mice received control IgG or α-PD-L1 from 5 d.p.t.i. % IFN-γ^{+} TILs (E) or % apoptotic TILs (F) from indicated groups at 16 d.p.t.i. (G) Tumor growth curves (n=5).

Representative data from 2 or 3 independent experiments except those data from pooled experiments. *$P \leq 0.05$, **$P \leq 0.01$, ***$P \leq 0.001$ (Student's t-test and Two-way ANOVA). See also Figure S4.

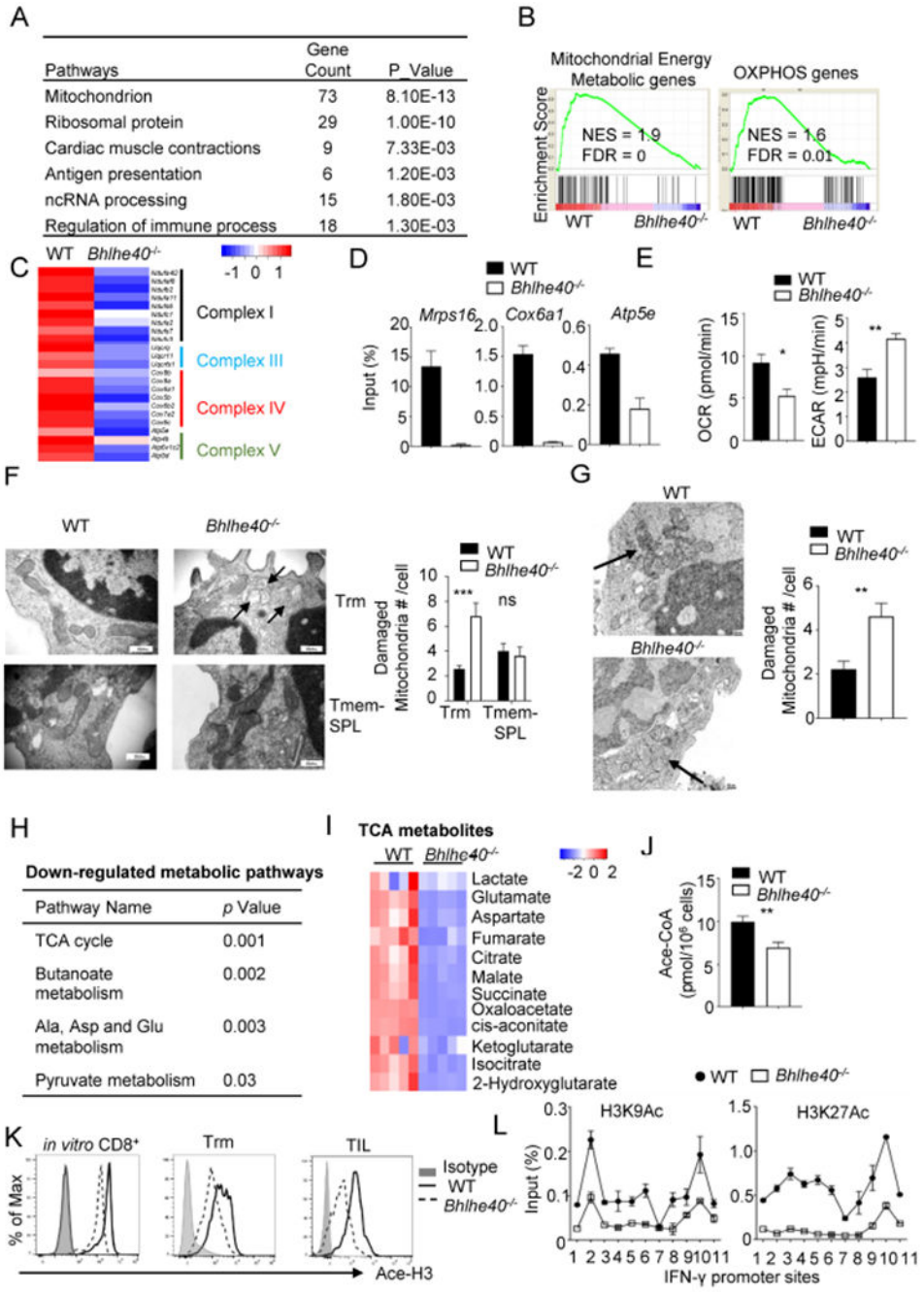

Figure 5. Bhlhe40 programs mitochondrial and epigenetic regulation of Trm cells and TILs

(A) WT or *Bhlhe40*$^{-/-}$ OTI cells were transferred into WT mice and infected with PR8-OVA. OTI Trm cells were sorted for RNA-seq at 42 d.p.i., KEGG pathway analysis of genes down-regulated in *Bhlhe40*$^{-/-}$ Trm cells.

(B) GSEA of mitochondrial energy metabolism or OXPHOS genes in WT vs. *Bhlhe40*$^{-/-}$ Trm cells.

(C) Heat map of mitochondrial complex gene expression in WT or *Bhlhe40*$^{-/-}$ Trm cells.

(D) Binding of Bhlhe40 to indicated mitochondrial genes in activated CD8^{+} T cells.

(E) Basal OCR or ECAR of WT or *Bhlhe40*$^{-/-}$ Trm cells at 42 d.p.i. (n= 3).
(F) Electron microscope (EM) images of mitochondria in WT or *Bhlhe40*$^{-/-}$ Trm or Tmem-SPL cells (scale bars,300 nm) (left). Damaged mitochondria counts per cell from each group (right).
(G) EM images of mitochondria in WT or *Bhlhe40*$^{-/-}$ TILs (scale bars, 200 nm) (left). Damaged mitochondria counts per cell from each group (right).
(H) Down-regulated metabolic pathways in *in vitro* activated *Bhlhe40*$^{-/-}$ CD8^{+} T cells compared to WT (4 d.p.a., n= 3).
(I) TCA cycle metabolites measured by GC/MS (concentration/million cells) in *in vitro* activated WT or *Bhlhe40*$^{-/-}$ CD8^{+} T cells (4 d.p.a.) (n=5).
(J) Acetyl-CoA concentrations in *in vitro* activated WT or *Bhlhe40*$^{-/-}$ T cells (4 d.p.a.) (n=6, 2 experiments).
(K) Acetyl-histone H3 of *in vitro* activated CD8^{+} T cells (4 d.p.a.), Trm cells (42 d.p.i.) or TILs (14 d.p.t.i.) from WT or *Bhlhe40*$^{-/-}$ mice (n=3-6).
(L) H3K9Ac (left) or H3K27Ac (right) at *Ifng* promoter were accessed by ChIP from *in vitro* activated CD8^{+} T cells (4 d.p.a.).
Representative data from 2 or 3 independent experiments except those data from pooled experiments and (A), (B), (G), (H) & (I). *$P \leq 0.05$,**$P \leq 0.01$ (Student's t-test). See also Figure S5.

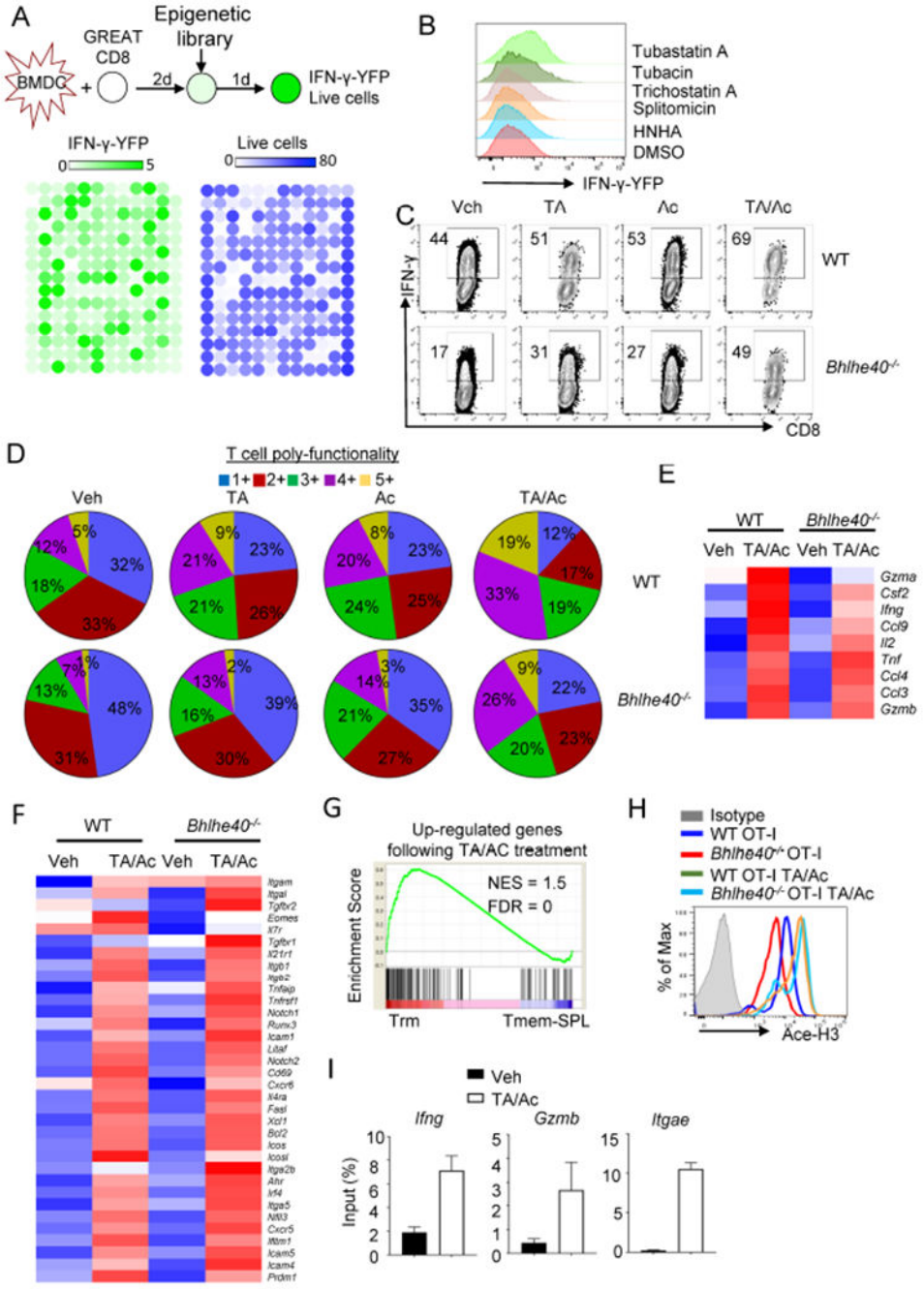

Figure 6. Identification of an epigenetic and metabolic regimen promoting CD8$^+$ T cell residency genes and functionality

(A) Schematics of epigenetic screening approach (top), heat map of IFN-γ-YFP fluorescence and cell viability of the T cells following screen (bottom).

(B) IFN-γ YFP expression following treatment of indicated epigenetic modifiers.

(C) % IFN-γ$^+$ CD8$^+$ T cells after treatment with vehicle (Veh), Tubastain A (TA), Acetate (Ac) or TA plus Ac (TA/Ac) at 3 d.p.a.

(D) Activated WT or *Bhlhe40*$^{-/-}$ CD8$^+$ T cells treated with Veh, TA, Ac or TA/Ac. The production of IFN-γ, TNF-α, GzmB, CCL3 and CCL4 was measured.

(E) Heat map of effector molecule genes in WT or *Bhlhe40*$^{-/-}$ CD8^{+} T cells (4 d.p.a.) following Veh or TA/Ac treatment (by Nanostring).
(F) Heat map of genes associated with Trm cell and TIL residency in WT or *Bhlhe40*$^{-/-}$ CD8^{+} T cells (4 d.p.a.) following Veh or TA/Ac treatment (by Nanostring).
(G) GSEA of upregulated genes shared by WT and *Bhlhe40*$^{-/-}$ CD8^{+} T cells after TA/Ac treatment (> 1.5 fold) in WT Trm vs. Tmem-SPL.cells
(H) Activated WT or *Bhlhe40*$^{-/-}$ OTI cells were treated with or without TA/Ac. Ace-H3 was measured in indicated groups.
(I) H3K9Ac at *Ifng, Gzmb* and *Itgae* promoter with or without TA/Ac treatment *in vitro* at 4 d.p.a.
Representative data from 2 or 3 independent experiments except (E), (F) & (G). See also Figure S6.

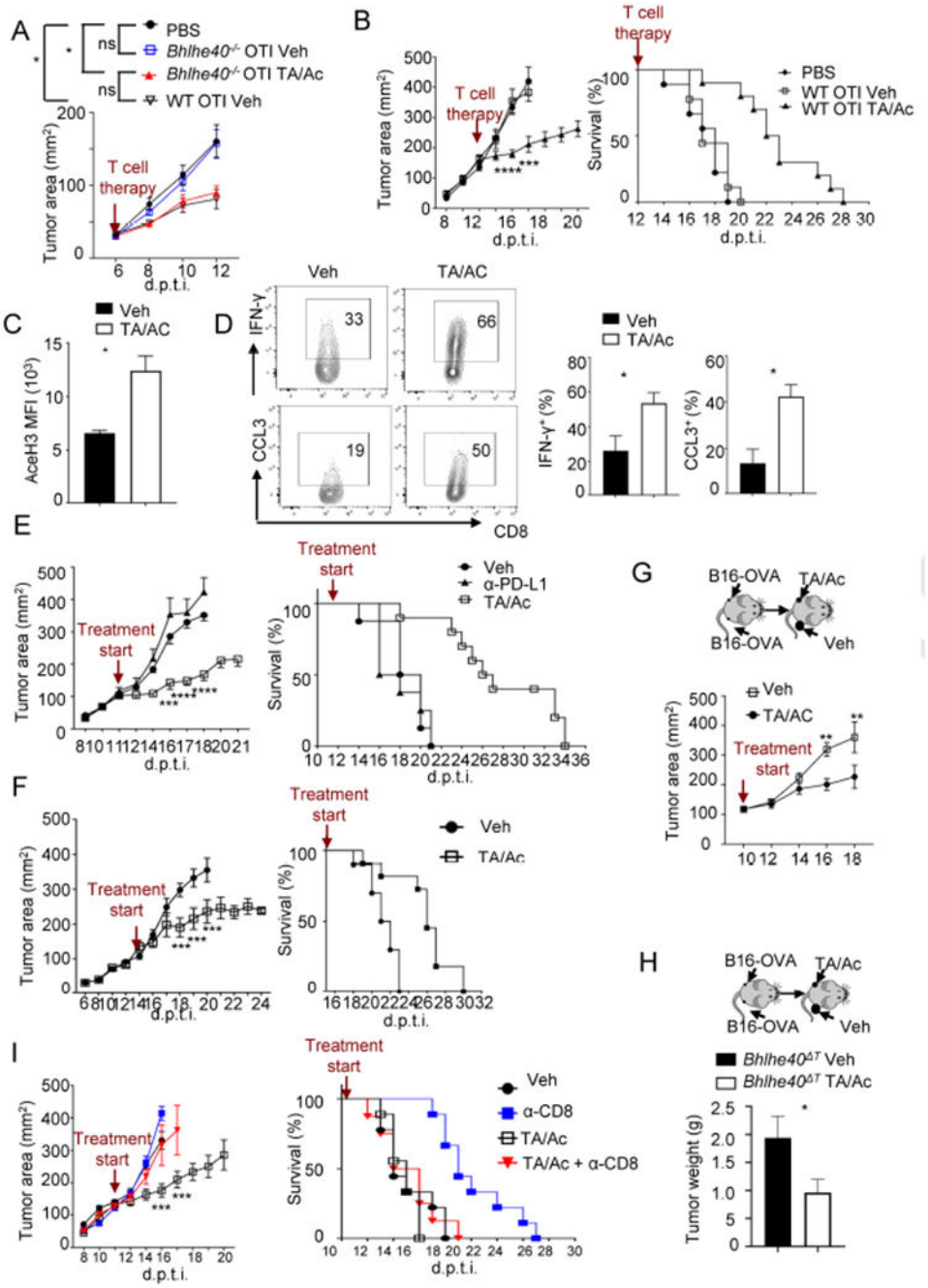

Figure 7. Tubastatin A and acetate treatment promotes antitumor activities of CD8$^+$ T cells

(A) B16-OVA bearing WT mice received PBS, WT effector OTI cells, *Bhlhe40*$^{-/-}$ effector OTI cells treated with Veh or TA/Ac at 6 d.p.t.i. (tumor < 45 mm^2). Tumor growth curves (n= 6-12, 2 experiments).

(B) B16-OVA bearing WT mice received PBS, WT effector OTI cells treated with Veh or TA/Ac at 12 d.p.t.i (tumor > 120 mm^2). Tumor growth and survival curves (n=9-10, 2 experiments).

(C, D) WT mice were treated with Veh or TA/Ac intratumorally from 11 d.p.t.i. (tumor > 100 mm^2). MFI of acetylated histone H3 (C), and % IFN-γ^+ or $CCL3^+$ cells (D) in TILs at 13 d.p.t.i. (n=3).

(E) B16-OVA growth and survival curves of mice that received intratumoral injection with α-PD-L1, Veh or TA/Ac from 11 d.p.t.i. (tumor > 100 mm^2) (n=8).

(F) MC38 growth and survival curves of mice that received intratumoral Veh or TA/Ac injection from 15 d.p.t.i. (tumor > 100 mm^2) (n=10, 2 experiments).

(G) B16-OVA were implanted into both sides of flank of WT mice followed with intratumoral injection of TA/Ac or Veh to one side at 10 d.p.t.i. Tumor growth curves of the two sides (n=6).

(H) B16-OVA were implanted into both sides of flank of *Bhlhe40*$^{\Delta T}$ mice followed with intratumoral injection of TA/Ac or Veh to one side at 10 d.p.t.i. Tumor weight of the two sides at 15 d.p.t.i. (n=6).

(I) B16-OVA growth and survival curves of mice that received anti-CD8a or IgG at 1 day before intratumorally injection of Veh or TA/Ac from 11 d.p.t.i. (tumor > 100 mm^2) (n=5-9, 2 experiments).

Representative data from 2 or 3 experiments except those data from pooled experiments and H. *$P \leq 0.05$,**$P \leq 0.01$, ***$P \leq 0.001$, ****$p < 0.0001$ (Student's t-test and Two-way ANOVA). See also Figure S7.

KEY RESOURCES TABLE

REAGENT or RESOURCE	SOURCE	IDENTIFIER
Antibodies		
APC/Cy7 anti-mouse CD8a Antibody	BioLegend	Cat. No. 100714, RRID: AB_312753
FITC anti-mouse CD8b Antibody	BioLegend	Cat. No. 126606, RRID: AB_961295
PerCP/Cyanine5.5 anti-mouse CD45 Antibody	BioLegend	Cat. No. 103132, RRID: AB_893340
PE anti-rat CD90/mouse CD90.1 (Thy-1.1) Antibody	BioLegend	Cat. No. 202524, RRID: AB_1595524
APC anti-mouse CD90.2 (Thy-1.2) Antibody	BioLegend	Cat. No. 140312, RRID: AB_10640728
Brilliant Violet 711™ anti-mouse CD279 (PD-1) Antibody	BioLegend	Cat. No. 135231, RRID: AB_2566158
Brilliant Violet 421™ anti-mouse CD366 (TIM-3) Antibody	BioLegend	Cat. No. 119723, RRID: AB_2616908
PerCP/Cyanine5.5 anti-mouse CD152 Antibody	BioLegend	Cat. No. 106316, RRID: AB_2564474
PE/Cy7 anti-mouse CD103 Antibody	BioLegend	Cat. No. 121426, RRID: AB_2563691
Brilliant Violet 510™ anti-mouse CD103 Antibody	BioLegend	Cat. No. 121423, RRID: AB_2562713
FITC anti-mouse CD69 Antibody	BioLegend	Cat. No. 104506, RRID: AB_313109
PE Anti-Mouse IFN gamma	BioLegend	Cat. No. 505808, RRID: AB_315402
Brilliant Violet 510™ anti-mouse TNF-α Antibody	BioLegend	Cat. No. 506339, RRID: AB_2563127
Pacific Blue™ anti-human/mouse Granzyme B Antibody	BioLegend	Cat. No. 515408, RRID: AB_2562196
CCL3 (MIP-1 alpha) Monoclonal Antibody (DNT3CC), eFluor 660, eBioscience™	ThermoFisher	Cat. No. 50-753282, RRID: AB_2574295
CCL4 (MIP-1 beta) Monoclonal Antibody (FL34Z3L), PerCP-eFluor 710, eBioscience™	ThermoFisher	Cat. No. 46-754042, RRID: AB_2573845
Ki-67 Monoclonal Antibody (SolA15), PE-Cyanine7, eBioscience™	ThermoFisher	Cat. No. 25-569882, RRID: AB_11220070
PE/Cy7 anti-human CD8a Antibody	BioLegend	Cat. No. 300914, RRID: AB_314118
Brilliant Violet 421™ anti-human CD279 (PD-1) Antibody	BioLegend	Cat. No. 329920, RRID: AB_10960742
PE anti-human CD11 a Antibody	BioLegend	Cat. No. 301208, RRID: AB_314146
Brilliant Violet 605™ anti-human CD45RO Antibody	BioLegend	Cat. No. 304238, RRID: AB_2562153
InVivoMAb anti-mouse PD-L1 (B7-H1)	BioXCell	Cat. No. BE0101 RRID: AB_10949073
InVivoMAb anti-mouse CD3ε	BioXCell	Cat. No. BE0261 RRID: AB_2687740
InVivoMAb anti-mouse CD28	BioXCell	Cat. No. BE0015-5 RRID: AB_1107628
InVivoMAb polyclonal Rat IgG	BioXCell	Cat. No. BE0094
Anti-acetyl-Histone H3 Antibody	Millipore	Cat. No. 06-599
Anti-ATP citrate lyase antibody	abcam	Cat. No. ab40793
PE Donkey anti-rabbit IgG (minimal x-reactivity) Antibody	BioLegend	Cat. No. 406421 RRID: AB_2563484
DEC1 Antibody	NOVUS	Cat. No. NB100-1800
Anti-Histone H3 (acetyl K9) antibody	abcam	Cat. No. ab4441
Anti-Histone H3 (acetyl K27) antibody	abcam	Cat. No. ab4729
Bacterial and Virus Strains		
Influenza A/PR8/34	Laboratory of Thomas Braciale	(Sun et al., 2011; Sun et al., 2009)

REAGENT or RESOURCE	SOURCE	IDENTIFIER
Influenza A/X-31	Laboratory of Thomas Braciale	(Sun et al., 2011)
Influenza A/PR8-OVA	Laboratory of Thomas Braciale	
Biological Samples		
Tumor tissue and PBMC from RCC patients	Mayo Clinic,	https://www.mayoclinic.org/
Tumor tissue and PBMC from RCC patients	Vanderbilt University Medical Center	https://ww2.mc.vanderbilt.edu/
Chemicals, Peptides, and Recombinant Proteins		
Influenza NP_{366} Tetramer	NIH Tetramer Facility	Cat# H-2D(b) ASNENMETM
Influenza PA_{224} Tetramer	NIH Tetramer Facility	Cat# H-2D(b) SSLENFRAYV
OVA_{257} Tetramer	NIH Tetramer Facility	Cat# H-2K(b) SIINFEKL
Collagenase Type 2	Worthington Biochemical	Cat# LS004177
Fetal Bovine Serum	HyClone	Cat# SH30070.03
RPMI 1640	GIBCO	Cat# 11875-093
Dulbecco's modified Eagle's medium	Corning	Cat# 10-017-CV
Penicillin-Streptomycin-Glutamine (10,000 U/mL)	GIBCO	Cat# 10378-016
Phosphate-Buffered Saline, 1X	Corning	Cat# 21-040-CV
On-Column DNase I Digestion Set	Sigma-Aldrich	Cat# DNASE70
FTY720	Cayman Chemical	Cat# 10006292
Corning™ Cell-Tak Cell and Tissue Adhesive	Corning™	Cat# CB40240
Monensin Solution (1,000X)	BioLegend	Cat# 420701
Influenza A NP (366 - 374) Strain A/NT/60/68 ASNENMDAM	Anaspec	Cat# AS-60623
OVA (257 - 264) SIINFEKL	Anaspec	Cat# AS-60193-5
Lung Dissociation Kit, mouse	Miltenyibiotec	Cat# 130-095-927
Tumor Dissociation Kit, mouse	Miltenyibiotec	Cat# 130-096-730
CD8a (Ly-2) MicroBeads, mouse	Miltenyibiotec	Cat# 130-117-044
Sodium acetate trihydrate	Sigma-Aldrich	Cat# S7670
Tubastatin A	Selleckchem	Cat# S8049
Sodium Pyruvate (100 Mm)	GIBCO	Cat# 11360070
Sodium citrate dihydrate	Sigma-Aldrich	Cat# W302600
Epigenetics Screening Library	Cayman	Cat# 11076 Batch# 04980804
Recombinant Mouse IL-1β (carrier-free)	BioLegend	Cat# 575106
Recombinant Mouse IL-15 (carrier-free)	BioLegend	Cat# 566304
Recombinant Mouse IL-21 (carrier-free)	BioLegend	Cat# 574506
Recombinant Mouse IL-7 (carrier-free)	BioLegend	Cat# 577806
Recombinant Mouse IL-33 (carrier-free)	BioLegend	Cat# 580506
Recombinant Mouse TNF-α (carrier-free)	BioLegend	Cat# 575206
Recombinant Mouse TGF-β1 (carrier-free)	BioLegend	Cat# 763104
Recombinant Mouse IL-10 (carrier-free)	BioLegend	Cat# 575806

REAGENT or RESOURCE	SOURCE	IDENTIFIER
Prostaglandin E2 (PGE2)	R&D systems	Cat# 2296/10
Critical Commercial Assays		
GenElute™ Mammalian Total RNA Miniprep Kit	Sigma-Aldrich	Cat# RTN350
RNeasy Mini Kit	QIAGEN	Cat# 74104
Fast SYBR Green Master Mix	Applied Biosystems	Cat# 4385612
M-MLV Reverse Transcriptase	Invitrogen	Cat# 28025-021
eBioscience™ Foxp3 / Transcription Factor Staining Buffer Set	Thermo Fisher Scientific	Cat# 00-5523-00
Intracellular Staining Permeabilization Wash Buffer (10X)	BioLegend	Cat# 420801
Fixation Buffer	BioLegend	Cat# 421002
nCounter® Mouse Immunology Panel	NanoString Technologies	Cat# XT-CSO-MIM1-12
PrimeFlow™ RNA Assay Kit	ThermoFisher	Cat# 88-18005-210
CellEvent™ Caspase-3&7 Green Flow Cytometry Assay Kit	ThermoFisher	Cat# C10427
Dimethyl α-ketoglutarate	Sigma Aldrich	Cat# 349631
Methyl pyruvate	Sigma Aldrich	Cat# 371173
SODIUM PYRUVATE (13C3, 99%)	Cambridge Isotope Laboratories	Cat# CLM-2440-0.5
L-GLUTAMINE (13C5, 99%)	Cambridge Isotope Laboratories	Cat# CLM-1822-H-0.1
Acetyl CoA Assay Kit	abcam	Cat# ab87546
Seahorse XFe/p FluxPaks	Agilent	Cat# 102340-100 103022-100
Seahorse XF Cell Mito Stress Test Kit	Agilent	Cat# 103015-100
ATP Determination Kit	ThermoFisher	Cat# A22066
Deposited Data		
Raw and analyzed RNA-seq data	This paper	GEO: GSE135278
Single cell RNA-seq of T cells in colorectal cancer	Zhang et al., 2018	EGAS00001002791
RNA-seq of Trm cell of lung from human	Hombrink et al., 2016	GEO: GSE61397
Experimental Models: Cell Lines		
B16-OVA	Laboratory of Haidong Dong	(Dronca et al., 2016)
MC38	Laboratory of Haidong Dong	(Tang et al., 2018)
LLC	Laboratory of Haidong Dong	
Experimental Models: Organisms/Strains		
C57BL/6J	The Jackson Laboratory	Cat# 000664
CD90.1 (Thy 1.1)	The Jackson Laboratory	Cat# 000406
OT-I	The Jackson Laboratory	Cat# 003831
CD4-Cre	The Jackson Laboratory	Cat# 017336
Flp	The Jackson Laboratory	Cat# 005703
Bhlhe40tm1a(KOMP)Wtsi	MMRRC	Cat# 88443
IFN-γ-YFP (GREAT)	The Jackson Laboratory	Cat# 017580
Bhlhe40$^{-/-}$	Laboratory of Brian T. Edelson	

REAGENT or RESOURCE	SOURCE	IDENTIFIER
Pdcd1$^{-/-}$	Laboratory of Haidong Dong	
Oligonucleotides		
Hprt-F: CTCCGCCGGCTTCCTCCTCA	This paper	
Hprt-R:ACCTGGTTCATCATCGCTAATC	This paper	
Acly-F: TTCGTCAAACAGCACTTCC	This paper	
Acly-R: ATTTGGCTTCTTGGAGGTG	This paper	
Bhlhe40 primers	IDT	Cat# Mm.PT.58.10417747
Cox6a1-F: ggtgctgtcagcgtctcggg	This paper	
Cox6a1-R: cgggtacctgaaccctcctcg	This paper	
Mrps16-F: cgtccgcaccactccagagcc	This paper	
Mrps16-R: gtagcagtcaaggatcagtc	This paper	
Atp5e-F: tttgcaatgtggttccatcg	This paper	
Atp5e-R: tcgagcccgctctgagtgac	This paper	
GzmB-F: ctgaatgctctccgctccct	This paper	
GzmB-R: gagtttggggtgaggggaaa	This paper	
Itgae-F: acttctggaagacagaaacc	This paper	
Itgae-R: caggcgggtctcagtgagtc	This paper	
Infg locus for Chip-PCR	Kabda et al.,2016 Peng et al., 2016	
Software and Algorithms		
GraphPad Prism 8	GraphPad Software	http://www.graphpad.com
FlowJo (version 10.5)	LLC	http://www.flowjo.com
nSolver 3.0	NanoString Technologies	http://www.nanostring.com/
R language		https://www.r-project.org/
GSEA	Broad Institute	http://software.broadinstitute.org/gsea/index.jsp